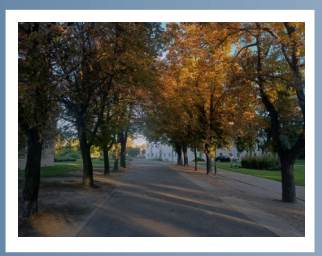

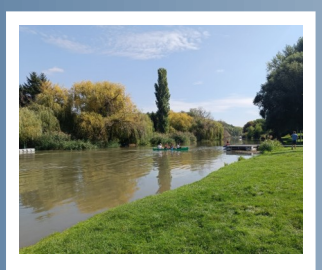

VOCAL2026

11th VOCAL Optimization Conference: Advanced Algorithms
Mosonmagyaróvár, Hungary
June 10-12, 2026

Short Papers

VOCAL 2026
11th VOCAL Optimization Conference: Advanced Algorithms

Mosonmagyaróvár, Hungary, June 10-12, 2026

Short Papers

Published by Faculty of Agricultural and Food Sciences, Széchenyi István University
Var tér 2, H-9200 Mosonmagyarovar, Hungary
E-mail: ovardekan@sze.hu
Website: https://ovarikar.sze.hu/en GB
Contact: Dr. Tamás Tóth, Dean of the Faculty
Single volume, electronic publication, format: pdf.

ISBN 978-615-6443-53-3

VOCAL 2026. 11th VOCAL Optimization Conference:
Advanced Algorithms. Mosonmagyaróvár, Hungary, June 10-12, 2026.
Short Papers

Contents

Application of a simple ALB model for the robotic assembly of an electronic device
Máté Csíkos and Tamás Koltai 4

Smoothing unadjusted Langevin algorithm for Kurdyka- Lojasiewicz potential functions
Susan Ghaderia, Yves Moreaua, and Masoud Ahookhoshb 10

Difference of high-order Moreau envelopes for DC optimization
Alireza Kabgani, Moslem Zamani, and Masoud Ahookhosh 16

Algorithms for Identifying the Crucial Decisions and Generating Strategic N-best Process Structures
Bertalan Kovács, Botond Bertók, and Márton Frits 22

Connecting Europe Through Hydrogen: Cost Allocation Analysis of Cross-Border Pipeline Coalition under Varying Subsidy Policies
Emmanuel Kwesi Arthur, Sofía De-León Almaraz, and Tamás Solymosi . 28

QUBO formulations for minimizing breaks in sports timetabling
Levente Gegő and Viktória Nemkin 34

Global convergence of scaled Polyak subgradient method for robust phase retrieval
Morteza Rahimi and Masoud Ahookhosh 41

On Bregman–Moreau envelope reformulations of DC programs
Moslem Zamani, Morteza Rahimi, and Masoud Ahookhosh 47

Bounds and exact values of some domination parameters on cylindrical graphs
Janez Žerovnik 53

Application of a simple ALB model for the robotic assembly of an electronic device

Máté Csíkos[1], Tamás Koltai[2]

[1] Juli Automation Europe Kft., Kecskemet, Hungary
m.csikos@juli-eu.com
[2] Management and Corporate Economics, Budapest University of Technology and Economics, Budapest, Hungary
koltai.tamas@gtk.bme.hu

Abstract. This study examines optimization in medium- and large-batch production, focusing on task allocation to reduce costs and cycle times. While prior research emphasizes algorithmic complexity of assembly line balancing (ALB) optimization problems, industrial automation demands more flexible and rapidly applicable modelling approaches. A case study of a high-precision optical document reader assembly line demonstrates the application of a Simple Assembly Line Balancing Problem (SALBP-2). An Integer Linear Programming (ILP) model is used to minimize cycle time in a dual-workstation setup typical of small- to medium-lot high-tech manufacturing. The results show that simplified, decision-oriented models—when properly adapted for robotic systems—can significantly improve throughput and resource utilization.

Keywords: Assembly line balancing (ALB), Integer linear programming, Operations management, Case study

1 Introduction

Assembly Line Balancing (ALB) partitions tasks into workstations to optimize costs, station number, or cycle times. The literature distinguishes between SALBP-1 (minimizing stations for fixed cycle time) and SALBP-2 (minimizing cycle time for fixed number of stations). Early research prioritized developing integer programming (IP) formulations for these NP-hard problems and finding techniques to cope with algorithmic complexity. Modern research has transitioned toward General Assembly Line Balancing Problems (GALBP), incorporating real-world complexities such as industrial robotics [3, 5]. While automation increases precision and volume, full automation is often unviable for small lot sizes, leading to hybrid systems and human-robot collaboration (HRC) [8]. Previous studies have explored human skill variability [6] and robotic integration [7], yet a critical dimension remains under-addressed: specific technological time constraints inherent in high-tech assembly.

In processes involving adhesives or coatings, task sequences are governed not only by precedence but also by dry times (mandatory minimum delays) and process open times (maximum quality windows). This paper extends ALB modelling by incorporating these constraints into a SALBP-2 framework through a case study of a

passport reader assembly line. The manufacturing of these optical devices relies on sensitive bonding where temporal synchronization is vital for success.

The novelty of this research is summarized in the following points:

1. Mathematical Integration of Technological Constraints: We propose a framework to include minimum (dry) and maximum (open) time gaps between tasks within a standard ALB model.

2. Managerial Implications: Analyzing trade-offs between technological requirements and optimal throughput.

The paper is structured as follows: Section 2 details the mathematical formulation of the applied model. Section 3 introduces the production environment and the parameters of the analyzed process. Section 4 summarizes the results while Section 5 discusses the management implication of the applied modelling approach. Finally, Section 6 concludes the study.

2 Model Formulation

To provide a formal framework for the assembly line balancing problem, the following notations and definitions are applied. A unique index i (i=1,…,I) is assigned to each tasks. A task may be identified by either its descriptive name or its index. Tasks that have no succeeding operations are defined as last tasks, and their indices are grouped in the set L. Similarly, workstations are indexed by j, j=1,…,J). J denotes the maximum number of workstations.

The core of the optimization lies in the assignment of tasks to specific workstations, which is represented by the binary decision variable x_{ij}. This variable is defined as follows: x_{ij}=1 if task I is assigned to workstation j otherwise x_{ij}=0.

Based on these definitions, the integer linear programming (ILP) formulation of the SALBP-2 model used in this study is presented below. The applied notations are summarized in Table 1.

The applied mathematical integer linear programing (MILP) model is as follows,

$$Min\ T_c \tag{1}$$

$$\sum_{i=1}^{I} t_i x_{ij} \leq T_c \qquad j = 1, \dots, J \tag{2}$$

$$\sum_{j=1}^{J} x_{ij} = 1 \qquad i = 1, \dots, I \tag{3}$$

$$\sum_{j=1}^{J} j\left(x_{qj} - x_{pj}\right) \geq 0 \qquad (p, q) \in P \tag{4}$$

$$\sum_{i \in V} t_i - d_{rs} \geq 0 \qquad (r, s) \in R \tag{5}$$

$$o_{tu} - \sum_{i \in W} t_i \geq 0 \qquad (t, u) \in T \tag{6}$$

The objective function (1) minimizes the cycle time. The left-hand side of equation (2) expresses the station time as a function of the assignment variables. The station time must be smaller than or equal to the cycle time which is minimized in (1). According

to equation (3), each task must be allocated exactly to one station. Constraint (4) ensures that all precedence relations among the tasks are satisfied.

Constraint (5) incorporates the dry time requirements, specifying that the difference between the sum of task times on the shortest path between tasks r and s and the mandatory dry time must be greater than or equal to zero (ensuring a minimum required delay). Finally, constraint (6) defines the process open time requirements, ensuring that the difference between the maximum allowable open time and the sum of task times on the longest path between tasks t and u remains greater than or equal to zero (ensuring the maximum window is not exceeded)

Table 1. Summary of notations.

Indices:		
i	-	index of tasks (i=1,…,I),
j	-	Index of robot stations (j=1,…,J).
Parameters:		
I	-	number of tasks,
J	-	number of robot stations,
t_i	-	time necessary to perform task i (task time),
s_j	-	time necessary to perform all tasks at station j (station time),
d_{rs}	-	dry time between tasks r and s, $(r, s) \in R$,
o_{tu}	-	open time between tasks t and u, $(t, u) \in T$.
Sets:		
P	-	set of index pairs which pertain to tasks with precedence relations, that is, $(p, q) \in P$ if task p immediately precedes task q.
R	-	set of index pairs which pertain to tasks with dry time connection, that is, $(r, s) \in R$ if task r precedes task s and requires dry times.
T	-	set of index pairs which belong to tasks with open time connection, that is, $(t, u) \in T$ if task t precedes task u, including open time,
V	-	set of indexes of those tasks which are on the shortest path within tasks r and s,
W	-	set of indexes of those tasks which are on the longest path within tasks t and u.
Variables:		
T_c	-	cycle time,
x_{ij}	-	assignment variable. If x_{ij}=1, task i is assigned to station j, otherwise x_{ij}=0.

3 ALB Models of the passport reader Manufacturer

3.1 Task Aggregation

To ensure model robustness and technological coherence, an initial task aggregation was conducted. By grouping operations that require specific grippers or specialized tooling, 430 elementary steps were synthesized into 14 high-level task groups. This reduction minimizes non-value-added material handling and ensures that logically interdependent operations remain at the same workstation.

In industrial practice, line configuration is dictated by target cycle times, categorized into four strategic magnitudes:

- *Long Cycle Times (~180s+)*: Stationary workpiece layout for high-complex, low-volume products like turbines or aircraft.
- *Medium Cycle Times (~45–180s)*: Standard move-on-completion models utilizing robotic or manipulator-based transfers (e.g., automotive body shops).
- *Short Cycle Times (~12-45s)*: Rigid automation with high-speed conveyors or AGV systems, common in electronics manufacturing
- *Ultra-short Cycle Times (<12s)*: Dedicated, cam-driven automated lines where throughput demands override flexibility (e.g., food industry).

It is important to emphasize that these threshold values serve as order-of-magnitude guidelines. The precise parameters for optimization are ultimately governed by the Design for Assembly (DfA) and Design for Manufacturing (DfM) principles and the specific manufacturing technologies deployed.

The assembly process is characterized by daily lot sizes ranging from 50 to 150 units. While most components are sourced from external suppliers, the Printed Circuit Board Assembly (PCBA) is performed in-house. For the purposes of this study, the PCBA stage is treated as an internal supply source, and potential synchronization issues are considered outside the scope of this model. Beyond standard assembly, the process includes specialized operations such as thermal paste dispensing, sealing, and adhesive bonding.

Table 2. Tasks and precedence relations of the sample problem.

i	Task	Task time i [s]	Prec. of task i
1	Thermal paste dispersion	8.9	-
2	Installing mirror, LED panels	96.8	-
3	Plasma-coating, gluing glass	84.54	-
4	Cover plate	16.31	-
5	Motherboard, connectors screwing	42.4	2
6	Shield screwing	51.8	3
7	Inner frame screwing	113.6	1, 5
8	Installing RF antenna	5.8	7
9	Sealing side house	39.2	6
10	Marriage	8.8	8, 9
11	Screwing	79.2	10
12	Attaching legs	15.2	11
13	Laser marking	19.9	12
14	End of line test	81.4	13

The primary objective is to minimize the cycle time for a given configuration of two workstations, which are represented by industrial robots in this study. To ensure operational feasibility, the assembly process was decomposed into 14 task groups based on expert engineering analysis indicated in Table 2.

The precedence relationships between the tasks presented in Table 2 are illustrated in Fig. 1.

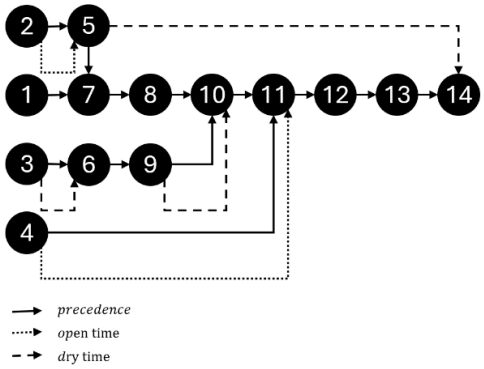

Fig. 1. Precedence relations between tasks with dry and open time.

4 Analysis of Optimization Results and Technological Constraints

The SALBP-2 model was evaluated against a solution proposed by experts based on simple heuristics. With 663.85 second work content, the process follows Long Cycle Time (~180s+) and fixed-position layout logic. The optimal solution of ILP model resulted in a 385.85 second cycle. This optimal solution outperforming the 389.6 second heuristic solution. This ~1% gain acts as compound interest, providing a more efficient baseline for refinement and significant long-term throughput increases.

Technological constraints do not require a departure from the SALBP-2 framework. Dry times function as mandatory buffer tasks, while open times are managed by localizing interdependent tasks within a single robot workstation. This internal sequencing eliminates inter-station transfers, minimizing quality risks.

Due to the small sample size, the computational time to reach the optimal solution was insignificant. However, as tasks and workstations scale upward, the combinatorial nature of ILP models increases computational intensity. Investigating these optimization thresholds for larger datasets remains a subject of future research.

5 Management and Practical Implications

Mathematical optimization is essential even in long-cycle environments where human intuition is often deemed sufficient. From an end-user perspective, knowing the mathematical optimum is crucial for managerial decisions; it either validates that human intuition was correct or reveals overlooked constraints. This benchmark

provides objective justification for line deployments, ensuring throughput is not lost to blind spots. The ILP model's superiority (385.85s vs. 389.6s) proves that combinatorial complexity persists after engineering aggregation. Expertise, such as that within Juli Automation Europe Kft., is most effectively utilized during initial task grouping, while mathematical modeling should finalize distribution to ensure maximum efficiency.

6 Conclusion and Summary

This research applied the SALBP-2 framework to a high-precision, long-cycle robot workstation setup. By synthesizing 430 micro-tasks into 14 groups, we established an industrially relevant ILP model.

The core contribution is empirical evidence that mathematical optimization yields measurable improvements (3.75s reduction) even in complex, low-volume scenarios. This 1% gain provides a foundation for cumulative efficiency and stability. The study validates the 'Magnitude-Based Balancing' approach, proving that high-tech efficiency results from strategic task grouping and mathematical refinement, supported by the industrial background of Juli Automation Europe Kft.

References

1. Baybars, I.: A Survey of Exact Algorithms for the Simple Assembly Line Balancing Problem. Management Science 32: 909–932. (1986).
2. Bowman, E. H.: Assembly Line Balancing by Linear Programming. Operations Research 8: 385–389. (1960)
3. Boysen, N., M. Fliedner, and A. Scholl.: Assembly Line Balancing: Which Model to Use When? International Journal of Production Economics 111: 509–528. (2008)
4. Bryton, B.: Balancing of a Continuous Production Line. Unpublished M.S. thesis, Northwestern University, Evanston, IL. (1954)
5. Helms, E., Schraft, R.D., Hagele, M.: rob@work: robot assistant in industrial environments. In: IEEE ROMAN 2002, 11th IEEE International Workshop on Robot and Human Interactive Communication, Berlin, Germany, pp. 399–404. (2002)
6. Koltai, T., Tatay, V. and Kalló N.: Application of the results of simple assembly line balancing models in practice: the case of a bicycle manufacturer (2013)
7. Koltai, T., Dimény, I., Gallina, V., Gaal, A. and Sepe, C.: An analysis of task assignment and cycle times when robots are added to human-operated assembly lines, using mathematical programming models (2021)
8. Krüger, J., T. K. Lien., and A. Verl.: Cooperation of human and machines in assembly lines CIRP Annals Volume 58, Issue 2: 628–646. (2009)
9. Salveson, M. E.: The Assembly Line Balancing Problem. Journal of Industrial Engineering 6: 18–25. (1955)
10. Scholl, A., and C. Becker.: State-of-Art Exact and Heuristic Solution Procedures for Simple Assembly Line Balancing. European Journal of Operational Research 168: 666–693. (2006)
11. Weckenborg, C., Kieckh¨ afer, K., Müller, C., Grunewald, M., Spengler, T.S.: Balancing of assembly lines with collaborative robots. Business Research 13, 93–132. (2019)

Smoothing unadjusted Langevin algorithm for Kurdyka-Łojasiewicz potential functions

Susan Ghaderi[a], Yves Moreau[a], and Masoud Ahookhosh[b]

[a] Department of Electrical Engineering ESAT-STADIUS, KU Leuven, Kasteelpark Arenberg 10, Leuven, 3001, Belgium, [b]Department of Mathematics, University of Antwerp, Antwerp, Belgium susan.ghaderi@kuleuven.be

Abstract. This paper builds on the theoretical foundation of the smoothing unadjusted Langevin algorithm (SULA), focusing on its ability to sample from posterior distributions that involve nonsmooth potential functions. Specifically, we study functions of the composite form $f + g$, where f is L-smooth and g is weakly convex. We first generate a smooth variant of the potential via forward-backward envelope and establish a non-asymptotic convergence of the sequence generated by SULA under the Kurdyka-Łojasiewicz (KL) condition. To demonstrate the practical value of these theoretical results, we apply SULA to matrix completion problems, an area where weak convexity is a common structural feature. Our numerical experiments back up the theoretical claims, highlighting SULA's effectiveness in this key application.

Keywords: Bayesian learning· Smoothed Unadjusted Langevin Algorithm· Forward–backward envelope · Kurdyka-Łojasiewicz inequality

1 Introduction

Sampling from high-dimensional distributions in statistical and machine learning, and specifically in Bayesian inference, is a challenging task due to the nature of the target distribution. Let us consider *sampling* from a canonical target distribution $\pi(x) : \mathbb{R}^p \to [0, \infty)$ given by

$$\pi(x) = \frac{e^{-\mathcal{U}(x)}}{\int_{\mathbb{R}^p} e^{-\mathcal{U}(y)} dy}, \tag{1.1}$$

where $\mathcal{U} : \mathbb{R}^p \to \mathbb{R}$ is a convex, nonsmooth, and measurable function, called the potential function, i.e.,

$$\int_{\mathbb{R}^p} \exp\{-\mathcal{U}(y)\} dy < +\infty.$$

Methodologies based on Bayesian inference are among the most popular methods to design a proper target distribution, called the posterior distribution, for the unknown parameters of a mathematical model by considering the prior beliefs on the parameters and the likelihood function of the given data set. Imposing prior

beliefs on the parameters allows modulating the uncertainty on those parameters by taking into account prior knowledge about the problem. This is accounted for by Bayes' rule via

$$\pi(x|D) \propto P(D|x)P(x),$$

where $D \in \mathbb{R}^{n\times p}$ is a given data set, $x \in \mathbb{R}^p$ is the parameter to be estimated, $\pi(x|D)$ is the posterior distribution, $P(D|x)$ is the likelihood function, and $P(x)$ is the prior distribution. Hence, the potential function of the problem (1.1) will be of the form $\mathcal{U}(x) := \log \pi(x|D) \propto \log P(D|x) + \log P(x)$. For the sake of simplicity, we set here $f(x) := \log P(D|x)$ and $g(x) := \log P(x)$, which leads to composite potential functions of the form $\mathcal{U}(x) = f(x) + g(x)$.

Markov chain Monte Carlo (MCMC) methods allow sampling from such a high-dimensional complex distribution, by providing ways to design a Markov chain whose *stationary equilibrium distribution* is $\pi(x)$. Under reasonable assumptions, the distribution of the successive samples of the Markov chain will converge to its equilibrium distribution. To further accelerate MCMC methods, one may combine them with gradient-based techniques. In particular, the Langevin stochastic differential equation is defined as

$$dx_t = -\nabla\overline{\mathcal{U}}(x_t) + \sqrt{2p}\mathcal{B}_t, \tag{1.2}$$

where $\{\mathcal{B}_t\}_{t\geq 0}$ is a p-dimensional Brownian motion. It has $\pi(x)$ as its stationary distribution, and its formulation allows sampling methods to use discretization and gradient-based techniques. Applying the Euler-Maruyama discretization scheme to SDE (1.2) leads to the discrete-time Markov chain $\{x_k\}$ given by

$$x_{k+1} = x_k - \gamma_{k+1}\nabla\overline{\mathcal{U}}(x_k) + \sqrt{2\gamma_{k+1}}\mathcal{Z}_k, \quad k \in \mathbb{N}, \tag{1.3}$$

where $\{\gamma_k\}_{k\geq 0}$ is a sequence of step-sizes that can be a constant or a vanishing sequence, and $\{\mathcal{Z}_k\}_{k\geq 0}$ is a sequence of independent and identically distributed (i.i.d.) standard n-dimensional Gaussian random variables.

In this study, we extend the theoretical understanding of ULA by establishing convergence under the *Kurdyka–Łojasiewicz (KL) inequality* [**?**] for nonsmooth potentials. We first generate a smooth version of the potential function via forward-backward envelope (FBE) [1,2,3], and assume FBE satisfies the following Kurdyka-Łojasiewicz inequality (see, e.g., [5] and reference therein):

Definition 1.1 (Kurdyka-Łojasiewicz inequality) *Let $h : S \to \mathbb{R}$ be a function defined on open set $S \subseteq \mathbb{R}^p$ with $h^* = \inf_{x\in S} h(x)$ and let the set of minimizers $X^* = \{x \in S \mid h(x) = h^*\}$ to be nonempty. The function f is said to satisfy the Łojasiewicz gradient inequality if for any critical point x^*, there exist constants $\kappa, \delta > 0$ and $\vartheta \in (0, 1)$ such that*

$$|h(x) - h^*|^\vartheta \leq \kappa\|\nabla h(x)\|, \quad \forall x \in \mathbb{R}^p. \tag{1.4}$$

Then, we present a smoothing version of the ULA algorithm (SULA) for sampling from (1.1) thanks to the smoothing properties of FBE. Next, we assume the KL inequality for FBE and provide a convergence rate of SULA.

2 Unadjusted Langevin algorithm via FBE

In this paper, we consider a nonsmooth composite potential function $\mathcal{U} : \mathbb{R}^p \to \mathbb{R}$ such that

$$\mathcal{U}(x) = f(x) + g(x), \tag{2.1}$$

where f is a smooth convex function, g is proper, convex, and lower semicontinuous (lsc), and $\mathcal{U}$ has a non-empty set of minimizers, i.e., $\arg\min \mathcal{U} \neq \emptyset$.

Throughout this paper, we suppose (2.1) satisfies the following assumptions:

(H1) $f : \mathbb{R}^n \to \overline{\mathbb{R}}$ is L_f-smooth (smooth with Lipschitz continuous gradients), i.e.,

$$\|\nabla f(x) - \nabla f(y)\| \leq L_f \|x - y\|. \tag{2.2}$$

(H2) $g : \mathbb{R}^n \to \overline{\mathbb{R}}$ is an extended real-valued, proper, weakly convex, and lsc function.

It follows from (H1) that

$$\mathcal{U}(z) \leq f(x) + \langle \nabla f(x), z - x \rangle + g(z) + \frac{1}{2\lambda}\|z - x\|^2, \qquad \lambda < 1/L_f,$$

which motivates the definition of the so-called forward–backward mapping, i.e.,

$$\mathcal{T}_\lambda^{f,g}(x) := \underset{z \in \mathbb{R}^p}{\arg\min} \left\{ f(x) + \langle \nabla f(x), z - x \rangle + g(z) + \tfrac{1}{2\lambda}\|z - x\|^2 \right\} \tag{2.3}$$

$$= \operatorname{prox}_{\lambda g}(x - \lambda \nabla f(x)). \tag{2.4}$$

where $\operatorname{prox}_{\lambda g}$ is the proximal operator of the function g. Analogous to the Moreau envelope [7], the forward–backward envelope has been introduced to generate a smooth variant of composite functions [1,2,?], which is given by

$$\mathcal{U}_\lambda^{f,g}(x) := \inf_{z \in \mathbb{R}^p} \left\{ f(x) + \langle \nabla f(x), z - x \rangle + g(z) + \tfrac{1}{2\lambda}\|z - x\|^2 \right\}. \tag{2.5}$$

The FBE preserves the minimizers of the original objective U and, under mild assumptions on g (convexity, weak convexity, or prox-regularity), is continuously differentiable, where its gradient can be expressed as

$$\nabla \mathcal{U}_\lambda^{f,g}(x) = Q_\lambda(x) R_\lambda(x), \quad Q_\lambda(x) = I - \lambda \nabla^2 f(x), \quad R_\lambda(x) = \tfrac{1}{\lambda}\big(x - \mathcal{T}_\lambda^{f,g}(x)\big).$$

Next, we assume that

(H3) $\mathcal{U}_\lambda^{f,g}$ satisfies the KL inequality with $\vartheta = \frac{1}{2}$.

and present a smoothing variant of the unadjusted Langevin algorithm via FBE, which we present in the following.

Algorithm 1 SULA (Smoothing Unadjusted Langevin Algorithm via FBE)

1: **Initialization** $x_0 \in \mathbb{R}^p$, $\lambda \in (0, 1/L_f)$, $\gamma \in (0, 1/L)$;
2: **while** stopping criteria do not hold **do**
3: Compute $\nabla \mathcal{U}_\lambda^{f,g}(x_k)$;
4: Set $x_{k+1} = x_k - \gamma \nabla \mathcal{U}_\lambda^{f,g}(x_k) + \sqrt{2\gamma}\mathcal{Z}_k$;
5: $k = k + 1$;
6: **end while**

Theorem 1 (Convergence of SULA with constant step-size). *Let the assumptions (H1)-(H3) hold. If $\{x_k\}_{k\geq 0}$ is generated by SULA (Algorithm 1) with constant step-size $\gamma \in (0, 1/L)$, then*

$$\mathbb{E}\Big[\mathcal{U}_\lambda^{f,g}(x_{k+1}) - \mathcal{U}_\lambda^{f,g}(x^*)\Big] \;\leq\; \Big(1 - \frac{\alpha}{\kappa^2}\Big)^{k+1} \mathbb{E}\left[\mathcal{U}_\lambda^{f,g}(x_0) - \mathcal{U}_\lambda^{f,g}(x^*)\right] + \frac{L\gamma p \kappa^2}{\alpha},$$

for $\alpha := \gamma\left(1 - \frac{L\gamma}{2}\right)$.

Proof. It follows from the L-smoothness of $\mathcal{U}_\lambda^{f,g}$ ([4, Theorem 1(vi)]) and Step 4 of SULA that

$$\begin{aligned}
\mathcal{U}_\lambda^{f,g}(x_{k+1}) &\leq \mathcal{U}_\lambda^{f,g}(x_k) + \left\langle \nabla \mathcal{U}_\lambda^{f,g}(x_k), x_{k+1} - x_k \right\rangle + \frac{L}{2}\|x_{k+1} - x_k\|^2 \\
&\leq \mathcal{U}_\lambda^{f,g}(x_k) - \gamma \left\langle \nabla \mathcal{U}_\lambda^{f,g}(x_k), \nabla \mathcal{U}_\lambda^{f,g}(x_k) \right\rangle + \sqrt{2\gamma} \left\langle \nabla \mathcal{U}_\lambda^{f,g}(x_k), \mathcal{Z}_k \right\rangle \\
&\quad + \frac{L}{2}\left\| -\gamma \nabla \mathcal{U}_\lambda^{f,g}(x_k) + \sqrt{2\gamma}\mathcal{Z}_k \right\|^2 \\
&= \mathcal{U}_\lambda^{f,g}(x_k) - \left(\gamma - \tfrac{L\gamma^2}{2}\right) \left\| Q_\lambda(x_k) \mathcal{R}_\lambda^{f,g}(x_k) \right\|^2 \\
&\quad + \sqrt{2\gamma}\,(1 - L\gamma) \left\langle Q_\lambda(x_k)\mathcal{R}_\lambda^{f,g}(x_k), \mathcal{Z}_k \right\rangle + L\gamma \|\mathcal{Z}_k\|^2.
\end{aligned}$$

Taking expectation from both sides of the latter inequality and using $E[\mathcal{Z}_k] = 0$, $E\left[\|\mathcal{Z}_k\|^2\right] = p$, and the uniform boundedness of $\nabla^2 f(\cdot)$ (i.e., $\|\nabla^2 f(\cdot)\| \leq L_1$), we come to

$$\begin{aligned}
\mathbb{E}\left[\mathcal{U}_\lambda^{f,g}(x_{k+1}) - \mathcal{U}_\lambda^{f,g}(x_k)\right] &\leq -\left(\gamma - \tfrac{L\gamma^2}{2}\right) \mathbb{E}\left[\left\|\nabla \mathcal{U}_\lambda^{f,g}(x_k)\right\|^2\right] \\
&\quad + \sqrt{2\gamma}\,(1 - L\gamma) \left\langle \nabla \mathcal{U}_\lambda^{f,g}(x_k), \mathbb{E}[\mathcal{Z}_k] \right\rangle + L\gamma \mathbb{E}\left[\|\mathcal{Z}_k\|^2\right] \\
&= -\left(\gamma - \tfrac{L\gamma^2}{2}\right) \mathbb{E}\left[\left\|\nabla \mathcal{U}_\lambda^{f,g}(x_k)\right\|^2\right] + L\gamma p.
\end{aligned}$$

Setting $\alpha := \gamma\left(1 - \frac{L\gamma}{2}\right)$, and subtracting $\mathcal{U}_\lambda^{f,g}(x^*)$ from both sides of the above inequality leads to

$$\begin{aligned}
\mathbb{E}\left[\mathcal{U}_\lambda^{f,g}(x_{k+1}) - \mathcal{U}_\lambda^{f,g}(x^*)\right] &\leq \mathbb{E}\left[\mathcal{U}_\lambda^{f,g}(x_k) - \mathcal{U}_\lambda^{f,g}(x^*)\right] \\
&\quad - \alpha \mathbb{E}\left[\left\|\nabla \mathcal{U}_\lambda^{f,g}(x_k)\right\|^2\right] + L\gamma p.
\end{aligned}$$

Here, using the Kurdyka-Łojasiewicz inequality (1.4) leads to

$$\mathbb{E}\left[\mathcal{U}_\lambda^{f,g}(x_{k+1}) - \mathcal{U}_\lambda^{f,g}(x^*)\right] \leq \left(1 - \frac{\alpha}{\kappa^2}\right) \mathbb{E}\left[\mathcal{U}_\lambda^{f,g}(x_k) - \mathcal{U}_\lambda^{f,g}(x^*)\right] + L\gamma p.$$

Now, by recursion, we get

$$\begin{aligned}
\mathbb{E}\left[\mathcal{U}_\lambda^{f,g}(x_{k+1}) - \mathcal{U}_\lambda^{f,g}(x^*)\right] &\leq \left(1 - \frac{\alpha}{\kappa^2}\right)^2 \mathbb{E}\left[\mathcal{U}_\lambda^{f,g}(x_{k-1}) - \mathcal{U}_\lambda^{f,g}(x^*)\right] \\
&\quad + L\gamma p\left(1 + \left(1 - \frac{\alpha}{\kappa^2}\right)\right) \\
&\leq \dots \\
&\leq \left(1 - \frac{\alpha}{\kappa^2}\right)^{k+1} \mathbb{E}\left[\mathcal{U}_\lambda^{f,g}(x_0) - \mathcal{U}_\lambda^{f,g}(x^*)\right] \\
&\quad + L\gamma p\left(1 + \dots + \left(1 - \frac{\alpha}{\kappa^2}\right)^k\right) \\
&\leq \left(1 - \frac{\alpha}{\kappa^2}\right)^{k+1} \mathbb{E}\left[\mathcal{U}_\lambda^{f,g}(x_0) - \mathcal{U}_\lambda^{f,g}(x^*)\right] + \frac{L\gamma p\kappa^2}{\alpha},
\end{aligned}$$

adjudicating our claim.

3 Application to matrix completion

Let us consider a data matrix $A \in \mathbb{R}^{m\times n}$ for which only a subset of entries indexed by $\Omega \subseteq \{1,\dots,m\} \times \{1,\dots,n\}$ is available. The goal of matrix completion is to recover the entire matrix, typically under the assumption that the underlying structure is low-rank. A common strategy is to introduce a factorization $A \approx UV^\top$, where $U \in \mathbb{R}^{m\times r}$ and $V \in \mathbb{R}^{n\times r}$ are low-dimensional factors. In order to both fit the observed entries and promote sparsity in the factors, one can formulate the following ℓ_1-regularized optimization problem:

$$\min_{U\in\mathbb{R}^{m\times r},\, V\in\mathbb{R}^{n\times r}} \ \frac{1}{2}\big\|\mathcal{P}_\Omega(A - UV^\top)\big\|_F^2 \ + \ \lambda\big(\|U\|_1 + \|V\|_1\big), \tag{3.1}$$

where $\mathcal{P}_\Omega$ denotes the orthogonal projection onto the set of observed entries, $\lambda > 0$ is a regularization parameter controlling sparsity, and $\|\cdot\|_1$ represents the entrywise ℓ_1-norm. In our experiments, we evaluate the proposed method on the standard MovieLens-100K dataset, which contains 100,000 user–item ratings with missing entries. SULA rapidly decreases the objective in early iterations and stabilizes with low test RMSE, indicating good generalization without overfitting.

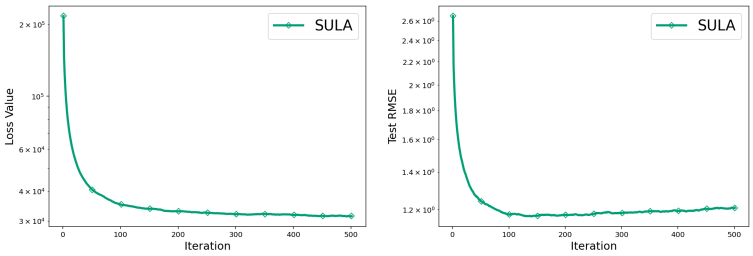

(a) Loss values rank 10.

(b) Test RMSE rank 10.

Fig. 1: Convergence behavior of SULA on the MovieLens-100K dataset.

4 Conclusion

In this study, we have proposed SULA, an unadjusted Langevin algorithm built upon the forward–backward envelope (FBE) smoothing technique, for sampling from nonsmooth potentials that satisfy the Kurdyka-Łojasiewicz inequality. The numerical results obtained from a matrix completion problem highlight the effectiveness of the proposed method, providing empirical support for the theoretical guarantees established in this work.

References

1. L. Stella, A. Themelis, and P. Patrinos, Forward–backward quasi-Newton methods for nonsmooth optimization problems, Computational Optimization and Applications, 67(3), 443-487, 2017.
2. A. Themelis, L. Stella, and P. Patrinos, Forward-backward envelope for the sum of two nonconvex functions: Further properties and nonmonotone linesearch algorithms, SIAM Journal on Optimization, 28(3), 2274-2303, 2018.
3. M. Ahookhosh, A. Themelis, and P. Patrinos, A Bregman forward-backward linesearch algorithm for nonconvex composite optimization: superlinear convergence to nonisolated local minima, SIAM Journal on Optimization, 31(1), 653-685, 2021.
4. S. Ghaderi, M. Ahookhosh, A. Arany, A. Skupin, P. Patrinos, and Y. Moreau, Smoothing unadjusted Langevin algorithms for nonsmooth composite potential functions, Applied Mathematics and Computation, 464, p. 128377, 2024.
5. M. Ahookhosh, S. Ghaderi, A. Kabgani, and M. Rahimi, Minimizing smooth Kurdyka–Łojasiewicz functions via generalized descent methods: Convergence rate and complexity, Optimization Theory and Applications, 2026.
6. S. Ghaderi, Y. Moreau, M. Ahookhosh, Unadjusted Langevin algorithm for sampling from Kurdyka-Łojasiewicz potential functions, Manuscript, KU Leuven, 2025.
7. J.J. Moreau, Proximité et dualité dans un espace hilbertien, Bulletin de la Société mathématique de France, 93, 273-299, 1965.

Difference of high-order Moreau envelopes for DC optimization

Alireza Kabgani, Moslem Zamani, and Masoud Ahookhosh

Department of Mathematics, University of Antwerp, Antwerp, Belgium
alireza.kabgani, Moslem.Zamani, masoud.ahookhosh@uantwerp.be

Abstract. We introduce the *high-order DC-envelope*, a smooth surrogate for difference-of-convex (DC) optimization obtained as the difference of the high-order Moreau envelopes of the two convex components. Building on recent advances in high-order proximal regularization, we show that the proposed envelope is continuously differentiable with a locally Lipschitz gradient, that its critical points are in one-to-one correspondence with DC-critical points of the original problem, and that its (local) minimizers recover (local) minimizers of the DC objective through a pair of high-order proximal evaluations. Exploiting this smooth reformulation, we propose an inexact two-prox gradient method on the high-order DC-envelope, prove an inexact descent inequality under a summable error model, and establish subsequential convergence to DC-critical points together with asymptotic recovery of primal minimizers. A scalar double-well experiment illustrates that, unlike the classical DCA, the proposed method with $p = 3$ can escape spurious local minima and reach the global solution.

Keywords: Difference-of-convex programming · High-order Moreau envelope · Proximal-point methods · Nonconvex optimization · DC-stationarity.

1 Introduction

Let us consider the unconstrained difference-of-convex (DC) problem

$$\min_{x\in\mathbb{R}^n} \varphi(x) := g(x) - h(x), \tag{1.1}$$

where $g, h : \mathbb{R}^n \to \overline{\mathbb{R}}$ are proper, lower semicontinuous, convex functions. The DC structure is remarkably expressive: a wide range of nonconvex objectives arising in sparse learning, robust statistics, signal processing, and image reconstruction can be cast in the form (1.1); see [5] for an extensive overview. The classical workhorse for (1.1) is the difference-of-convex algorithm (DCA) [5,7], which iteratively linearizes h and solves a convex surrogate. Refinements and accelerations have been proposed, including proximal DC schemes and boosted variants [6,8]. Although DCA enjoys monotone descent and weak convergence guarantees, it is, by construction, driven by a *purely local* model of h and is therefore prone to stagnation at the first DC-critical point encountered along its

trajectory. In landscapes with multiple basins, this typically means that DCA gets trapped in the local well that contains the initial iterate.

A complementary line of research, originating with the forward-backward envelope [9], exploits smooth surrogates of nonsmooth problems to enable gradient-type methods with stronger global behavior. In the same spirit, recent work has shown that replacing quadratic regularization in proximal-point methods by a high-order term $\frac{1}{p\gamma}\|\cdot\|^p$ with $p > 1$ leads to algorithms with improved complexity bounds and better practical behavior in nonconvex problems [1,2,3,4].

Motivated by this observation, we extend the envelope perspective from $p = 2$ to arbitrary $p > 1$. Our first contribution is conceptual: we define the *high-order DC-envelope* and show that it retains the essential stationary and minimization structure of the original DC problem. Our second contribution is algorithmic: we propose an inexact high-order two-prox method based on approximate proximal points of g and h, and prove an inexact descent inequality under a summable envelope-gradient error model. Finally, we present a compact numerical example showing that the higher-order geometry can matter in practice: for a scalar double-well DC objective, the case $p = 3$ escapes the attraction region where DCA and $p = 2$ stagnate.

Outline. Section 2 fixes notation and recalls the high-order proximal operator and Moreau envelope. Section 3 introduces the high-order DC-envelope and develops its variational properties. Section 4 presents the inexact two-prox method, its convergence analysis, and the numerical illustration.

2 Preliminaries and notation

We recall the high-order proximal operator (HOPE) and the high-order Moreau envelope (HOME) [2,3,4].

Definition 1. *Let $p > 1$, $\gamma > 0$, and $\psi : \mathbb{R}^n \to \overline{\mathbb{R}}$ be proper. The HOPE of ψ is*

$$\mathbf{prox}^p_{\gamma\psi}(x) := \operatorname*{\mathbf{arg\,min}}_{y\in\mathbb{R}^n} \left\{ \psi(y) + \frac{1}{p\gamma}\|x - y\|^p \right\}, \tag{2.1}$$

and the HOME of ψ is

$$\psi^{\gamma,p}(x) := \inf_{y\in\mathbb{R}^n} \left\{ \psi(y) + \frac{1}{p\gamma}\|x - y\|^p \right\}. \tag{2.2}$$

For proper lower semicontinuous convex ψ, the map $\mathbf{prox}^p_{\gamma\psi}(x)$ is single-valued and the envelope $\psi^{\gamma,p}$ is differentiable with

$$\nabla\psi^{\gamma,p}(s) = \frac{1}{\gamma} J_p\big(s - \mathbf{prox}^p_{\gamma\psi}(s)\big). \tag{2.3}$$

where for $p > 1$, $J_p(x) := \|x\|^{p-2}\, x$, with the convention $J_p(0) = 0$.

3 High-order difference of convex envelope (DCE)

We now introduce the high-order smoothing of the DC objective.

Definition 2. *For the DC objective $\varphi = g - h$, the high-order DC-envelope is defined as*

$$\mathbf{dce}_{\gamma,p}(s) := g^{\gamma,p}(s) - h^{\gamma,p}(s). \tag{3.1}$$

By (2.3), the envelope $\mathbf{dce}_{\gamma,p}$ is differentiable. If $u = \mathbf{prox}^p_{\gamma h}(s)$ and $v = \mathbf{prox}^p_{\gamma g}(s)$, then

$$\nabla \mathbf{dce}_{\gamma,p}(s) = \frac{1}{\gamma}\big(J_p(s-v) - J_p(s-u)\big). \tag{3.2}$$

For $p \geq 2$, this gradient is locally Lipschitz on every ball as shown below.

Lemma 1. $\mathbf{dce}_{\gamma,p}$ *is Lipschitz on* $\mathbf{B}(0;r)$ *for any* $r > 0$ *with a Lipschitz constant* $\mathcal{L}_E$*, i.e, for any* $\gamma > 0$*,* $p \geq 2$*, and* $r > 0$*,*

$$\|\nabla \mathbf{dce}_{\gamma,p}(x_2) - \nabla \mathbf{dce}_{\gamma,p}(x_1)\| \leq \mathcal{L}_E \|x_2 - x_1\|, \qquad \forall x_1, x_2 \in \mathbf{B}(0;r).$$

Definition 3. *A point* $\overline{x} \in \mathbf{dom}(g) \cap \mathbf{dom}(h)$ *is called DC-critical for* (1.1) *if* $\partial g(\overline{x}) \cap \partial h(\overline{x}) \neq \emptyset$*.*

We now show that DC-stationarity can be expressed by the coincidence of two high-order proximal points.

Theorem 1 (High-order proximal characterization of DC-stationarity). *Let* $\overline{x} \in \mathbf{dom}(g) \cap \mathbf{dom}(h)$*. The following are equivalent:*

(a) $\overline{x}$ *is DC-critical;*
(b) *there exist* $\gamma > 0$ *and* $\overline{s} \in \mathbb{R}^n$ *such that* $\overline{x} = \mathbf{prox}^p_{\gamma g}(\overline{s}) = \mathbf{prox}^p_{\gamma h}(\overline{s})$*;*
(c) *for every* $\gamma > 0$ *there exists* $\overline{s} \in \mathbb{R}^n$ *such that* $\overline{x} = \mathbf{prox}^p_{\gamma g}(\overline{s}) = \mathbf{prox}^p_{\gamma h}(\overline{s})$*.*

The envelope also admits a useful comparison with the original DC objective.

Theorem 2. *Let* $s \in \mathbb{R}^n$*, and define* $u = \mathbf{prox}^p_{\gamma h}(s)$ *and* $v = \mathbf{prox}^p_{\gamma g}(s)$*. Then*

$$\varphi(v) \leq \mathbf{dce}_{\gamma,p}(s) \leq \varphi(u). \tag{3.3}$$

Theorem 3. *Let* $u = \mathbf{prox}^p_{\gamma h}(s)$ *and* $v = \mathbf{prox}^p_{\gamma g}(s)$*. Then the following are equivalent:*

(a) $\nabla \mathbf{dce}_{\gamma,p}(s) = 0$*;*
(b) $u = v$*;*
(c) u *is DC-critical for* (1.1)*.*

Thus, minimizing the envelope is compatible with minimizing the original DC function.

Theorem 4. *Let* $S_\star := \operatorname*{\mathbf{arg\,min}}_{s\in\mathbb{R}^n} \mathbf{dce}_{\gamma,p}(s)$. *Then*

$$\operatorname*{\mathbf{arg\,min}}_{x\in\mathbb{R}^n} \varphi(x) = \mathbf{prox}^p_{\gamma h}(S_\star) = \mathbf{prox}^p_{\gamma g}(S_\star), \tag{3.4}$$

and $\mathbf{inf}_{x\in\mathbb{R}^n}\varphi(x) = \mathbf{inf}_{s\in\mathbb{R}^n}\mathbf{dce}_{\gamma,p}(s)$.

We also record the local counterpart.

Theorem 5. *For* $s\in\mathbb{R}^n$, *set* $u(s) := \mathbf{prox}^p_{\gamma h}(s)$ *and* $v(s) := \mathbf{prox}^p_{\gamma g}(s)$.

(a) *Let* $x^\star$ *be a local minimizer of* φ, *and suppose there exists* $\xi^\star \in \partial g(x^\star)\cap \partial h(x^\star)$. *Define*

$$s^\star := x^\star + \gamma^{q-1} J_q(\xi^\star), \qquad q := \frac{p}{p-1}.$$

Then $s^\star$ *is a local minimizer of* $\mathbf{dce}_{\gamma,p}$, *and* $\mathbf{dce}_{\gamma,p}(s^\star) = \varphi(x^\star)$.

(b) *Let* $s^\star$ *be a local minimizer of* $\mathbf{dce}_{\gamma,p}$, *and define* $x^\star := u(s^\star)$. *Assume in addition that* $\mathbf{prox}^p_{\gamma h}$ *is locally surjective at* $s^\star$, *i.e., there exist neighborhoods* U *of* $s^\star$ *and* V *of* $x^\star$ *such that* $V\subseteq \mathbf{prox}^p_{\gamma h}(U)$. *Then* $x^\star$ *is a local minimizer of* φ.

4 Inexact high-order two-prox method

Let $\widetilde{u}^k, \widetilde{v}^k$ be approximate solutions of the two high-order proximal subproblems:

$$\widetilde{u}^k \approx \mathbf{prox}^p_{\gamma h}(s^k), \qquad \widetilde{v}^k \approx \mathbf{prox}^p_{\gamma g}(s^k),$$

and define the approximate envelope gradient

$$\widetilde{G}_k := \frac{1}{\gamma}\Big(J_p(s^k - \widetilde{v}^k) - J_p(s^k - \widetilde{u}^k)\Big), \tag{4.1}$$

Algorithm 1 Inexact high-order two-prox method

1: **Initialization** Start with $s^0\in\mathbb{R}^n$, $k=0$ and $\gamma>0$ and $p>1$;
2: **while** stopping criteria do not hold **do**
3: Compute $u^k \approx \mathbf{prox}^p_{\gamma h}(s^k)$ and $v^k \approx \mathbf{prox}^p_{\gamma g}(s^k)$ and update

$$s^{k+1} = s^k - \alpha_k \widetilde{G}_k. \tag{4.2}$$

4: $k = k+1$;
5: **end while**

To analyze (4.2), we impose an envelope-gradient error model.

Assumption 6 *There exists a sequence* $\{e^k\}_{k\in\mathbb{N}_0} \subseteq \mathbb{R}^n$ *such that*

$$\widetilde{G}_k = \nabla \mathbf{dce}_{\gamma,p}(s^k) + e^k, \qquad \sum_{k=0}^{\infty} \left\|e^k\right\|^2 < \infty. \tag{4.3}$$

Moreover, $\mathbf{dce}_{\gamma,p}(s)$ *is bounded below on* $\mathbb{R}^n$ *and the sequence* $\{s^k\}_{k\in\mathbb{N}_0}$ *generated by Algorithm 1 remains in a ball* $\mathbf{B}(0;r)$.

Theorem 7. *Let Assumption 6 satisfies. Suppose that the step sizes satisfy* $0 < \underline{\alpha} \le \alpha_k \le \overline{\alpha} < \frac{3}{4\mathcal{L}_E}$ *for all* $k \in \mathbb{N}_0$. *Then there exist constants* $c_1 > 0$ *and* $C_1 > 0$ *such that*

$$\mathbf{dce}_{\gamma,p}(s^{k+1}) \le \mathbf{dce}_{\gamma,p}(s^k) - c_1 \left\|\nabla \mathbf{dce}_{\gamma,p}(s^k)\right\|^2 + C_1 \left\|e^k\right\|^2 \qquad \forall k \in \mathbb{N}_0. \tag{4.4}$$

Consequently,

$$\sum_{k=0}^{\infty} \left\|\nabla \mathbf{dce}_{\gamma,p}(s^k)\right\|^2 < \infty, \qquad \nabla \mathbf{dce}_{\gamma,p}(s^k) \to 0. \tag{4.5}$$

Theorem 8. *Let Assumption 6 satisfies. Then every cluster point* $\overline{s}$ *of* $\{s^k\}_{k\in\mathbb{N}_0}$ *generated by Algorithm 1 satisfies* $\nabla \mathbf{dce}_{\gamma,p}(\overline{s}) = 0$. *If* $\overline{u} := \mathbf{prox}^p_{\gamma h}(\overline{s})$ *and* $\overline{v} := \mathbf{prox}^p_{\gamma g}(\overline{s})$, *then* $\overline{u} = \overline{v}$ *and this common point is DC-critical for* (1.1).

Theorem 9. *Suppose* $\{s^k\}_{k\in\mathbb{N}_0}$ *generated by Algorithm 1 satisfies* $\mathbf{dist}(s^k, S_\star) \to 0$. *For each* $k \in \mathbb{N}_0$, *define the exact proximal points* $u^k := \mathbf{prox}^p_{\gamma h}(s^k)$ *and* $v^k := \mathbf{prox}^p_{\gamma g}(s^k)$, *and let* $\widetilde{u}^k, \widetilde{v}^k \in \mathbb{R}^n$ *be approximate proximal points such that* $\left\|\widetilde{u}^k - u^k\right\| \to 0$ *and* $\left\|\widetilde{v}^k - v^k\right\| \to 0$. *Then*

$$\mathbf{dist}(u^k, \mathbf{arg\,min}\varphi) \to 0, \qquad \mathbf{dist}(v^k, \mathbf{arg\,min}\varphi) \to 0, \tag{4.6}$$

and

$$\mathbf{dist}(\widetilde{u}^k, \mathbf{arg\,min}\varphi) \to 0, \qquad \mathbf{dist}(\widetilde{v}^k, \mathbf{arg\,min}\varphi) \to 0. \tag{4.7}$$

Numerical illustration. We consider the scalar DC function $\varphi(x) = g(x) - h(x)$ with

$$g(x) = \frac{1}{4}(x^2-1)^2 + \frac{\tau}{2}(x-a)^2 + \lambda|x-x_g| + \lambda|x-x_\ell| + \frac{\kappa}{4}x^4, \qquad h(x) = \frac{\mu}{3}|x|^3 + \frac{\kappa}{4}x^4.$$

We choose $\tau = 0.4$, $a = -2$, $\mu = 2$, $\lambda = 3$, and $\kappa = 3$, with $x_g = -2.4$, $x_\ell = 2.1$, $s^0 = 1$, and $\gamma = 1$. For Algorithm 1, we use fixed step sizes $\alpha = 0.20$ for $p = 2$ and $\alpha = 0.35$ for $p = 3$ and all methods are run for 200 iterations.

This choice creates an asymmetric double-well landscape whose left basin contains the global minimizer. Figure 1 shows that DCA is attracted to the right-hand local well, while the case $p = 3$ crosses the barrier and converges to the deeper left-hand basin. The quadratic case $p = 2$ also moves leftward but much more slowly. This behavior is consistent with the geometry of the update: DCA uses a linearization of h, while Algorithm 1 follows the gradient of the high-order DC-envelope through the difference of two proximal points.

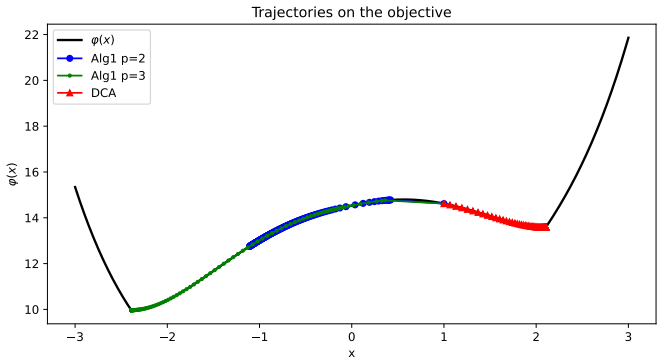

Fig. 1: Comparison of Algorithm 1 for $p = 2$ and $p = 3$ against DCA on the scalar double-well DC example. The higher-order model with $p = 3$ reaches the global well, while DCA and $p = 2$ remain inferior or slower.

References

1. Ahookhosh, M., Iusem, A., Kabgani, A., Lara, F.: Asymptotic convergence analysis of high-order proximal-point methods beyond sublinear rates. `https://doi.org/10.48550/arXiv.2505.20484`,
2. Ahookhosh, M., Nesterov, Y.: High-order methods beyond the classical complexity bounds: inexact high-order proximal-point methods. Mathematical Programming, **208**, 365–407 (2024).
3. Kabgani, A., Ahookhosh, M.: ItsOPT: An inexact two-level smoothing framework for nonconvex optimization via high-order Moreau envelope. `https://arxiv.org/abs/2410.19928`, (2025).
4. Kabgani, A., Ahookhosh, M.: Moreau envelope and proximal-point methods under the lens of high-order regularization. Set-Valued and Variational Analysis, **33**, 47 (2025)
5. Le Thi, H.A., Pham Dinh, T.: DC programming and DCA: thirty years of developments. Mathematical Programming **169**(1), 5–68 (2018)
6. Liu, T., Pong, T.K., Takeda, A.: A refined convergence analysis of pDCA$_e$ with applications to simultaneous sparse recovery and outlier detection. Computational Optimization and Applications **73**(1), 69–100 (2019)
7. Pham Dinh, T., Le Thi, H.A.: Convex analysis approach to D.C. programming: theory, algorithms and applications. Acta Mathematica Vietnamica **22**(1), 289–355 (1997)
8. Sun, K., Sun, X.A.: Algorithms for difference-of-convex programs based on difference-of-Moreau-envelopes smoothing. INFORMS Journal on Optimization **5**(4), 321–339 (2022)
9. Themelis, A., Hermans, B., Patrinos, P.: A new envelope function for nonsmooth DC optimization. In: 59th IEEE Conference on Decision and Control, pp. 4697–4702 (2020)

Algorithms for Identifying the Crucial Decisions and Generating Strategic N-best Process Structures

Bertalan Kovács, Botond Bertók, and Márton Frits

University of Pannonia, 8200 Veszprém, Egyetem u. 10, Hungary

Abstract. When synthesizing process networks, P-graph algorithms have the practical benefit of resulting in the N-best optimal and near-optimal process structures efficiently. However, the N-best often include a set of networks differing only marginally from the optimal one. For instance, two alternative routes between the same locations may differ only by a single turn. In contrast, in most applications, we expect alternative networks to be substantially different from each other. In multilevel optimization, strategic decisions at the upper levels substantially limit the availability of resources in the lower levels of alternative cases or constructive time periods. In most decision support systems the aim is to analyze N-best strategic decision alternatives instead of the N-best incomplete utilization of already available resources. In this work, first a modified branch and bound algorithm is proposed for efficient enumeration of the strategically N-best process networks by modifying both the decision variable selection and branching. Second, we propose an algorithm to identify those elements in the initial maximal structure whose inclusion or exclusion have significant consequences for the rest of the network, which can reduce the need for domain-specific knowledge when selecting strategic operating units. The proposed methods generate more diverse alternatives when synthesizing the N-best networks of a given process network synthesis problem and will be illustrated by case studies.

Keywords: Analysis and engineering of optimization algorithms

1 Problem

A significant limitation of current N-best approaches within the P-Graph framework [1] is the lack of structural diversity among top-ranked solutions. In larger networks, the best solutions are often nearly identical, differing only by a small number of low-impact operating units. As a result, many of the returned solutions provide little additional strategic insight. To address this, there is a need for a solver capable of generating N-best solutions that are meaningfully different, allowing decision-makers to evaluate a variety of structurally distinct yet near-optimal network architectures.

2 Expanding the model

The P-Graph model was extended to support the designation of operating units as **strategically important**. Such designations may be provided directly by domain experts when specific operating units correspond to high-level decisions, such as supplier selection in logistics networks, or equipment acquisition in process engineering applications. Alternatively, strategic importance can be determined automatically based on the structural properties of the network.

For automatic identification, an operating unit is considered strategically important if its removal results in a substantial reduction in the size of the maximal structure of the network. We use reduction in the size of the maximal structure as a proxy for strategic importance, as it reflects the extent to which an operating unit influences the availability of alternative network substructures. Such operating units are referred to as strategic units throughout the remainder of this paper. The size of a maximal structure ($|G_{\max}|$) is defined as the number of operating units present in the network generated by the MSG algorithm [3]. More formally, let $G_{\max}$ denote the maximal network and $G_{\max}^{-u}$ the maximal network obtained after removing operating unit u. Operating unit u is classified as strategically important when the relative decrease in network size exceeds a predefined threshold ($\frac{|G_{\max}|-|G_{\max}^{-u}|}{|G_{\max}|} \geq \delta$). This threshold is configurable and may be adjusted on a per-problem basis to account for differences in network connectivity and redundancy characteristics across application domains. No universally applicable threshold is currently known, and the appropriate value may depend on the structure of the underlying network.

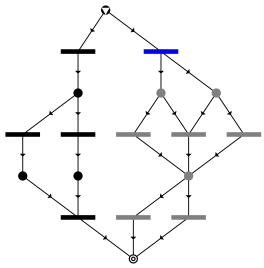

Fig. 1. The highlighted operating unit (blue) is identified to be strategically important, as it is the only operating unit creating materials used by the grey subnetwork.

2.1 Algorithmically determining strategically important units

To identify strategic units automatically, each operating unit is temporarily removed from the current solution and the resulting maximal structure is recom-

puted using the MSG algorithm. The relative reduction in network size is then evaluated according to the criterion defined in the previous section. Operating units exceeding the specified threshold are classified as strategically important.

During branch-and-bound search, the strategic importance of operating units may change as operating units are excluded from candidate solutions (see Figure 2). Therefore, strategic units can be recomputed whenever the excluded set grows. This improves adaptability but introduces additional computational overhead. As an alternative, strategic units may be identified once for the initial problem and kept fixed throughout the search, reducing runtime at the cost of potentially missing units that become important only in specific subproblems.

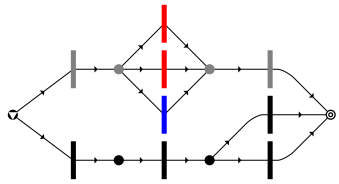

Fig. 2. Strategic importance may depend on the current subproblem. The highlighted unit (blue) becomes strategic after the alternative pathways (red) are excluded.

It should also be noted that the dynamic classification is inherently local to the current subproblem. The dynamically identified set of strategic units should be interpreted as reflecting the structure of the current subproblem rather than that of the original problem.

2.2 Branching strategy

We implemented an alternative branching strategy that explicitly exploits the identified strategic units. Whenever the maximal network associated with the current subproblem contains strategic units, the solver generates a branch for every feasible strategic choice, i.e., every feasible set of included strategic units. If n strategic units are present, this yields up to 2^n potential branches corresponding to all possible combinations of the strategic choices.

In practice, the number of strategic units is typically small and many strategic choices are infeasible. Consequently, only a fraction of the theoretical 2^n branches require examination. An example is shown in (Figure 3), where multiple strategic units correspond to alternative pathways within a common subnetwork.

This strategy is particularly beneficial in parallel search [4]. Although the same structural decisions would eventually be introduced by the standard branching procedure, explicitly branching on strategic units produces a larger set of structurally distinct subproblems near the root of the search tree. These subproblems can therefore be distributed among worker threads significantly faster.

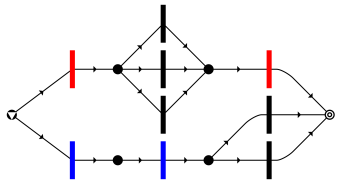

Fig. 3. Strategic units grouped into two dependent pairs. Units of the same color must either both be included or both excluded.

2.3 Saving solutions

To reduce redundancy among the found solutions, they are grouped according to their strategic choices. For each strategic choice, only the best solution found during the search is kept. The insertion procedure used to maintain this bounded solution pool is shown in Algorithm 1.

Algorithm 1 Insertion into the strategic solution pool

```
 1: procedure SaveSolution(solution, N)
 2:     S ← solution.stratSet
 3:     if S ∈ solutions then
 4:         if solution.value < solutions[S].value then
 5:             solutions[S] ← solution
 6:         end if
 7:     else
 8:         if |solutions| < N then
 9:             solutions[S] ← solution
10:         else
11:             worst ← Worst(solutions)
12:             if solution.value < worst.value then
13:                 Remove worst from solutions
14:                 solutions[S] ← solution
15:             end if
16:         end if
17:     end if
18: end procedure
```

2.4 Strategic Choice-Aware Lower Bounds

The original branch-and-bound implementation maintained a single global lower bound corresponding to the cost of the worst solution currently stored in the solution pool. If fewer than N solutions had been found, the lower bound was

treated as ∞. Since the relaxed cost associated with a subproblem provides an optimistic estimate of the best achievable cost of the final solution within that branch, any subproblem whose relaxed cost exceeded the current lower bound could be safely discarded.

The introduction of strategic choice-based solution storage enables a stronger pruning criterion. Since only a single solution is retained for each strategic choice, strategic choice-specific lower bounds can be used. If a solution with the same strategic choice has already been found, its cost is used as the lower bound. Only subproblems corresponding to previously unseen strategic choices continue to use the global lower bound. Algorithm 2 summarizes the resulting lower-bound computation.

This modification allows large portions of the search tree to be discarded earlier. Once a low-cost solution has been found for a particular strategic choice, subproblems with the same strategic choice are discarded unless they can improve upon the existing solution, reducing the number of subproblems that require detailed evaluation.

Algorithm 2 Strategic choice-aware lower bound

```
1: procedure LowerBound(S, N)
2:     if S ∈ solutions then
3:         return solutions[S].value
4:     else if |solutions| ≥ N then
5:         return Worst(solutions).value
6:     else
7:         return ∞
8:     end if
9: end procedure
```

3 Performance

The proposed approach was evaluated using a three-company case study introduced in [2]. The case study contains six strategic units corresponding to inter-company connections. The original study computed all the optimal networks for all feasible structures and grouped them by the solutions' strategic choices afterwards. The proposed solver reproduced the same set of solutions – while examining fewer network structures – confirming that the introduced branching, solution storage, and pruning strategies preserve the correctness of the search process.

Table 1 compares post-search filtering, strategic choice-based storage, and the proposed strategic choice-aware lower bound approach. Most of the observed improvement originates from the lower-bound pruning strategy introduced in Section 2.4, which reduces runtimes substantially. The proposed approach produces

the same 19 solutions as the original case study while reducing the runtime by up to 74% and the amount of network structures examined by 76%.

Table 1. Performance comparison on the three-company case study.

Method	Runtime (ms)	Structures Examined	Solutions
Post-search filtering	31718	139545	19*
Strategic choice-based storage	23476	97931	19
Strategic choice-aware lower bounds	8282	33669	19

4 Conclusions

This work extends the branch-and-bound based N-best P-graph solver to generate strategically distinct process networks. Strategic units are incorporated into branching, solution storage, and pruning, enabling the direct generation of solutions that differ in their strategic choices. The evaluated case study demonstrates that the proposed approach reproduces the same strategically distinct solutions as previous methods while substantially reducing search effort. A heuristic method for automatically identifying strategic units based on their impact on the maximal structure is also proposed. Future work will investigate alternative identification methods and evaluate the approach on larger industrial case studies.

References

1. Friedler, F., Tarjan, K., Huang, Y.W., Fan, L.T.: P-graphs for Process Systems Engineering: Mathematical Models and Algorithms. Springer, Cham (2022). https://doi.org/10.1007/978-3-030-92216-0
2. Orosz Ákos, Teng S.Y., Friedler F.: N-best Design Options with Strategical Differences in Process Network Synthesis, Chemical Engineering Transactions, 120, 409-414. (2025)
3. Friedler, F., Tarjan, K., Huang, Y.W., Fan, L.T.: Graph-theoretic approach to process synthesis: Polynomial algorithm for maximal structure generation. Comput. Chem. Eng. **17**(9), 929–942 (1993). https://doi.org/10.1016/0098-1354(93)80074-W
4. Varga, J.B., Friedler, F., Fan, L.T.: Parallelization of the accelerated branch-and-bound algorithm of process synthesis: Application in total flowsheet synthesis. Acta Chimica Slovenica **42**, 15–20 (1995)

* In total, 3083 solutions were found, which were then grouped by their strategic choices, resulting in 19 solutions.

Connecting Europe Through Hydrogen: Cost Allocation Analysis of Cross-Border Pipeline Coalition under Varying Subsidy Policies

Emmanuel Kwesi Arthur[1], Sofía De-León Almaraz[1], Tamás Solymosi[2,3]

[1]Corvinus University of Budapest, Institute of Operations and Decision Sciences, Department of Supply Chain Management, Fővám tér 8, 1093 Budapest, Hungary
[2]Corvinus University of Budapest, Institute of Operations and Decision Sciences, Department of Operations Research, Fővám tér 8, 1093 Budapest, Hungary
[3]Corvinus University of Budapest, Institute of Advanced Studies, Corvinus Center for Operations Research, Fővám tér 8, 1093 Budapest, Hungary
arthur.kwesi@stud.uni-corvinus.hu, de.sofia@uni-corvinus.hu, tamas.solymosi@uni-corvinus.hu

Abstract: One of EU's ambitious targets is to develop hydrogen (H_2) pipeline network of 53,000 km across the whole of Europe by 2040. The vision is to repurpose 60% of the existing gas pipelines and create 40% new pipelines that will transport green hydrogen from regions of abundance renewable energy sources potential to regions that require imports to meet their demand. While this vision, championed by European Hydrogen Backbone (EHB) promises the flow of 14M tonnes of low-carbon hydrogen energy within the continent, its infrastructure deployment requires huge capital costs. Subsidies are essential to de-risk such investments and to foster collaboration among EU countries and stakeholders. The absence of a coordinated pipeline may lock regions into localized hydrogen 'islands', limit trade, increase H_2 price volatility and slow down overall hydrogen economy. As a result, we model cross-border hydrogen pipeline development as a cooperative game theory with transferable utility to investigate how varying financial subsidy rates incentivize full cooperation. Maximum subsidy rates of 30% and 50% were adjusted exogenously for different coalition sizes to examine the grand coalition formation. We show that under progressive subsidy designs, grand coalition formation is beneficial to all players. Our work suggests that a uniform rate subsidy structure may inadvertently disincentivize cooperation by favoring bilateral agreements or smaller coalition groupings.

Keywords: Hydrogen Pipelines, European Hydrogen Backbone, Cost Allocation Games, Cooperative Game Theory.

1. Introduction

Studies show that hydrogen energy will account for about 18% of global energy demand by 2050 and will contribute to 20% of CO_2 emission reduction targets [1]. From 2020 to date, various initiatives with clear hydrogen targets have been presented to ensure this ambition is realized. One of such is the European Hydrogen Backbone's (EHB) vision to deploy hydrogen pipeline network infrastructure starting by 2030 [2]. The plan is to develop H_2 pipeline network of 31,500 km by 2030 and extend it to 53,000 km by 2040 with the vision to repurpose 60% of the existing gas pipelines and create 40% new pipelines that will transport green hydrogen from regions of abundance renewable energy sources (RES) potential to regions that require imports to meet their demand. This initiative involves local and international governments, regulatory bodies, private investors, etc., calling for cross border collaboration [3].

Subsidies are essential for de-risking investments and fostering collaboration among EU countries and stakeholders. The Regulation (EU) 2021/1153 (policy instrument) provides the legal framework that enables financial instruments, such as CEF to provide up to 50% grants of eligible CAPEX (for infrastructure co-financing) and up to 30% of total eligible cost (for transport cofinancing) for cross-border infrastructure projects like pipelines shared by multiple countries designated as PCIs [4]. Utilizing the cofinancing rates from the policy instrument, maximum subsidy rates of 30% and 50% were adjusted exogenously for different coalition sizes to examine the grand coalition formation. This paper investigates how varying financial subsidy rates incentivize full cooperation in H_2 pipeline infrastructure development and to examine how the costs (and savings) is allocated among countries to have stable and satisfactory coalitions.

2. Methodology

To assess the cooperative dynamics of hydrogen pipeline development, a 7-step methodology is proposed (Figure 1). In step 1, the HyCorridorE case study is developed, where the research scope and coalition countries are defined. Step 2 covers pipeline characterization and data collection, followed by Step 3: identification of a suitable game-theoretical model. Step 4 defines subsidy and simple rules scenarios. Step 5 discusses the verification of grand coalition stability. Step 6 involves calculations and analysis for the different scenarios, culminating in the discussion of the results in Step 7. The methodology is outlined in the figure below (Figure 1).

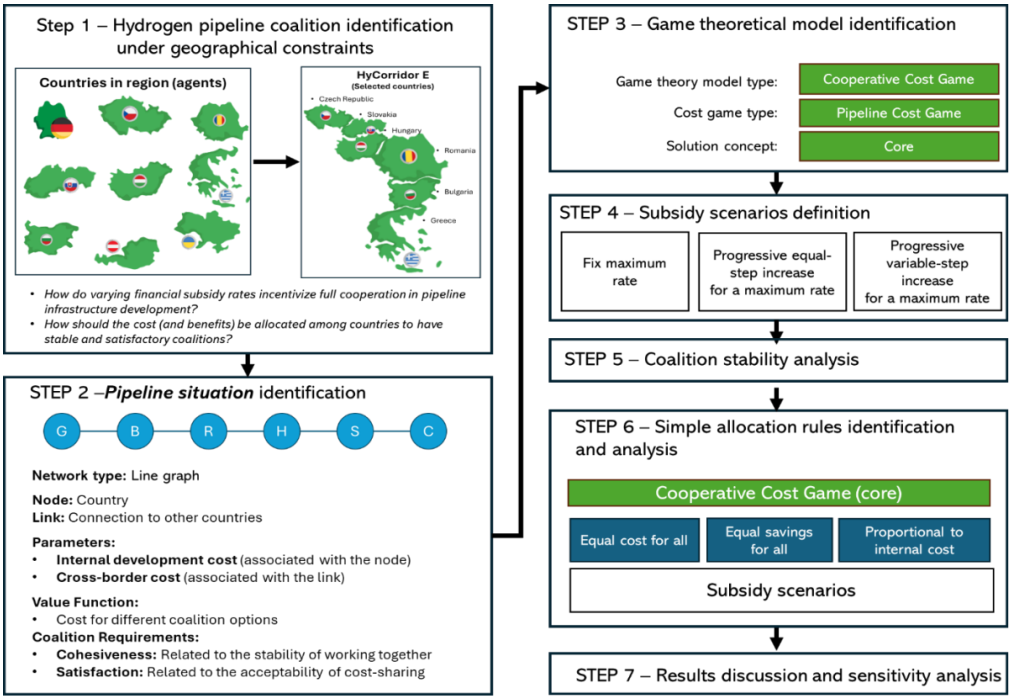

Figure 1: Methodology

This paper utilizes cooperative game theory to evaluate coalition risks under varying subsidy regimes in the development of hydrogen pipeline infrastructure. The "HyCorridor E" case, inspired by Corridor E from the

EHB [5] and the South-East European Hydrogen Corridor [6]. The HyCorridorE flows northward from Greece (G) through Bulgaria (B), Romania (R), Hungary (H), Slovakia (S), and into the Czech Republic (C), forming a linear route that shares one or two borders (Figure 2).

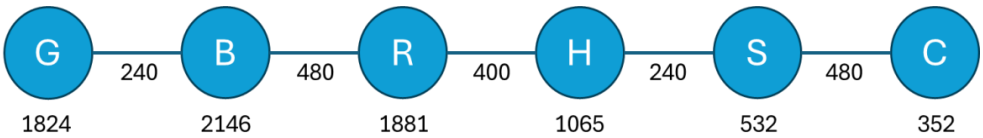

Figure 2. HyCorredorE pipeline situation with cost (M EUR) per node (internal cost) and link (cross-border cost).

In this study, a specific six-player cooperative cost game (N, c) is developed where the players in $N = \{1, 2, \dots, 6\}$ are countries arranged in a linear order that restricts realistic cooperation only to the $\frac{6(6+1)}{2} = 21$ (6 single-player and $\frac{6(6-1)}{2} = 15$ multi-player) connected (interval) coalitions. Although the function $c: 2^N \to R$, with $c(\emptyset) = 0$, specifies the cost for each of the $2^6 - 1 = 63$ non-empty coalitions, the costs of the $42 = 63 - 21$ non-interval coalitions contain no new information, these values are additively determined from the values of the 21 connected coalitions.

This game model is a special type of situation where the agents are positioned along a line graph that restricts cooperation to connected coalitions. The infrastructure development cost $d(S)$ of connected coalition S includes the costs incurred at the nodes (internal costs) and at the links (cross-border costs). However, towards the construction of the infrastructure of any connected coalition $S \subseteq N$, an external (or central) financing authority provides subsidies that reduce the actual infrastructure development costs $d(S)$ to a subsidized coalition cost

$$c(S) = (1 - r_s) \cdot d(S) \tag{1}$$

where r_s is the subsidy rate of the connected coalition S consisting of $s = |S|$ countries. Note that the subsidy rate depends only on the number of countries forming a connected coalition, regardless of their identities.

However, the costs depend on external subsidies; hence, collaboration of neighboring connected coalitions may not always be beneficial. In this pipeline cost game model, cohesiveness (any division of the grand coalition into interval coalitions should result in positive gains by merging) is a necessary and a sufficient condition for core non-emptiness (although in general cooperative game model, it is not).

Formally, Cost game (N, c) is called *cohesive*, if $c(N_1) + \cdots + c(N_k) \geq c(N)$ for all partitions $N_1 \cup \dots \cup N_k = N$ $(k \geq 2)$ of the *grand coalition* N. If cost game (N, c) is not cohesive because of, say, $c(S_1) + \cdots + c(S_k) < c(N)$ for some partition $S_1 \cup \dots \cup S_k$ of N, then for any allocation x, the inequality $f(S_1, x) + \cdots + f(S_k, x) < f(N, x) = 0$ holds, implying that at least one of the satisfactions $f(S_1, x), \dots, f(S_k, x)$ must be negative. The Component additivity of the coalitional cost function in the pipeline cost game (N, c) also implies that the core is already determined by the interval coalitions. Formally,

$$Core(N, c) = \{x \in \boldsymbol{R}^N : f(N, x) = 0 \text{ and } f(S, x) \geq 0 \text{ for all interval coalitions } S \neq \emptyset, N\} \tag{2}$$

Note that the cost game and its corresponding savings game are equivalent models of a cost-sharing situation; furthermore, the core allocations in the two games are in one-to-one correspondence given by simple linear coordinate transformations.

In the pipeline cost game, two subsidy regimes (fixed and progressive), allowing a maximum of 30% and

50% support are used based on EU regulation [4]. Three simple allocation rules: the equal cost, equal savings and cost shares proportional to internal cost, have been applied to the H_2 HyCorridorE pipeline situation.

3. Discussion

As explained in the methodology section, cohesiveness of the pipeline cost game (N, c) is required for the full cooperation to be beneficial. Figure 3 presents all 31 interval partitions with their gains by merging values from no cooperation (at the bottom) to full cooperation (at the top) for the two fixed subsidy rate designs. Since the gain by merging value is negative for at least one interval partition, the cost game is not cohesive; thus, the core is empty in both cases.

A: Max30%=fix30%

size (s)	subsidy rate r(s)											
						GBRHSC						
1	0											
2	0,3			G-BRHSC	GB-RHSC	GBR-HSC	GBRH-SC	GBRHS-C				
3	0,3			379,20	-336,00	-280,00	-168,00	-230,40				
4	0,3											
5	0,3	G-B-RHSC	G-BR-HSC	G-BRH-SC	G-BRHS-C	GB-R-HSC	GB-RH-SC	GB-RHS-C	GBR-H-SC	GBR-HS-C	GBRH-S-C	
6	0,3	687,00	99,20	211,20	148,80	-51,70	-504,00	-566,40	-128,50	-510,40	-238,80	
		G-B-R-HSC	G-B-RH-SC	G-B-RHS-C	G-BR-H-SC	G-BR-HS-C	G-BRH-S-C	GB-R-H-SC	GB-R-HS-C	GB-RH-S-C	GBR-H-S-C	
		971,30	519,00	456,60	250,70	-131,20	140,40	99,80	-282,10	-574,80	-199,30	
				G-B-R-H-SC	G-B-R-HS-C	G-B-RH-S-C	G-BR-H-S-C	GB-R-H-S-C				
				1122,80	740,90	448,20	179,90	29,00				
						G-B-R-H-S-C						
						1052,00						

B: Max50%=fix50%

size (s)	subsidy rate r(s)											
						GBRHSC						
1	0											
2	0,5			G-BRHSC	GB-RHSC	GBR-HSC	GBRH-SC	GBRHS-C				
3	0,5			792,00	-240,00	-200,00	-120,00	-64,00				
4	0,5											
5	0,5	G-B-RHSC	G-BR-HSC	G-BRH-SC	G-BRHS-C	GB-R-HSC	GB-RH-SC	GB-RHS-C	GBR-H-SC	GBR-HS-C	GBRH-S-C	
6	0,5	1625,00	592,00	672,00	728,00	500,50	-360,00	-304,00	212,50	-264,00	82,00	
		G-B-R-HSC	G-B-RH-SC	G-B-RHS-C	G-BR-H-SC	G-BR-HS-C	G-BRH-S-C	GB-R-H-SC	GB-R-HS-C	GB-RH-S-C	GBR-H-S-C	
		2365,50	1505,00	1561,00	1004,50	528,00	874,00	913,00	436,50	-158,00	414,50	
				G-B-R-H-SC	G-B-R-HS-C	G-B-RH-S-C	G-BR-H-S-C	GB-R-H-S-C				
				2778,00	2301,50	1707,00	1206,50	1115,00				
						G-B-R-H-S-C						
						2980,00						

Figure 3: Gains by merging of interval partitions under the fixed subsidy rate policies

Under the fixed rate subsidy (30% and 50%) strategies, the formation of the grand coalition is threatened. This type of strategy only promotes small-scale, but not full-scale cooperation towards the unified pipeline project. This is because once countries receive the fixed maximum subsidy in their smaller groups, they gain no additional financial incentive from merging. This suggests that a uniform rate subsidy structure may inadvertently disincentivize cooperation by favoring bilateral agreements or smaller groupings.

However, the considered progressive subsidy designs provide the desired cohesiveness, where merging is always beneficial. Figures 4a and 4b reveal that under all progressive subsidy regimes, the involvement of

Greece is necessary for cooperation to be beneficial, showing that Greece is a key H_2 supplier in the HyCorridorE pipeline development.

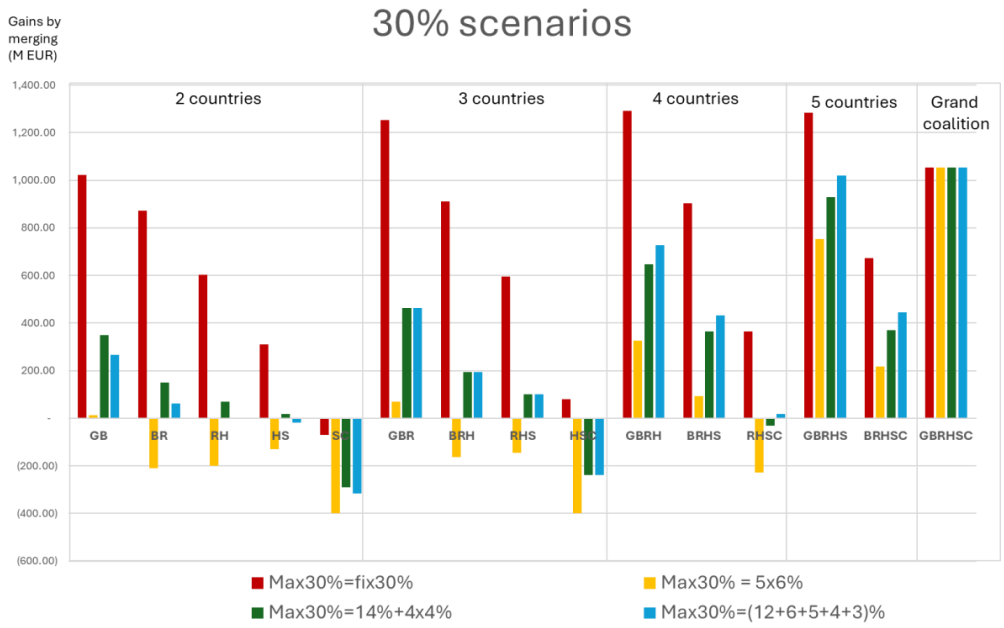

Figure 4a: Gains (savings) of coalitions under the max 30% subsidy scenarios

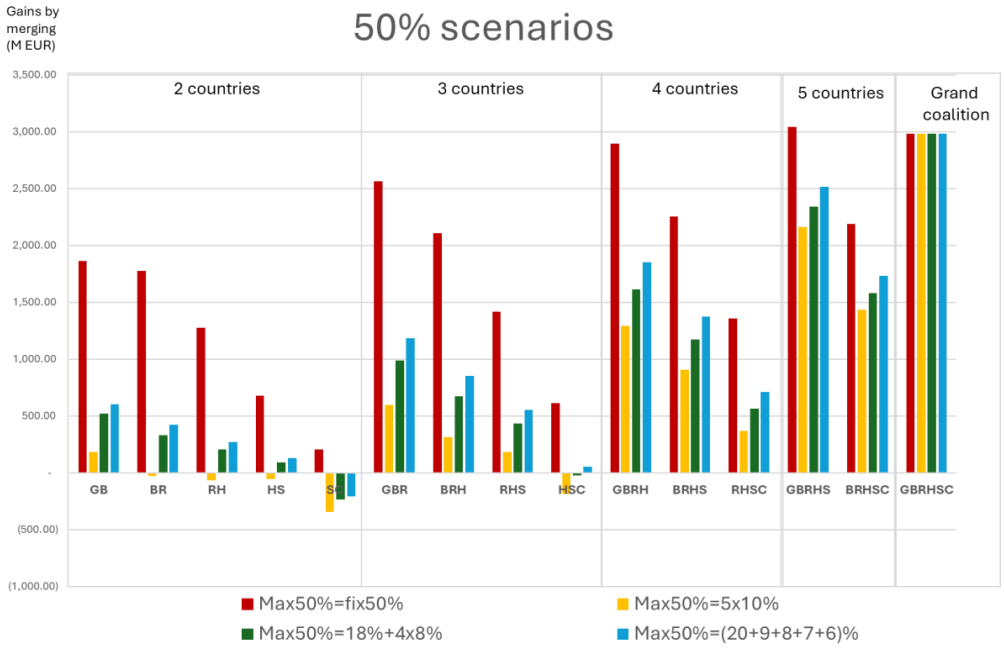

Figure 4b: Gains (savings) of coalitions under the max 50% subsidy scenarios.

4. Conclusions

Under the fixed subsidy design, there is an incentive to cooperate in smaller groups than in the grand coalition, indicating instability in the desired fully unified pipeline project. This policy regime may be easier to communicate but difficult to implement when the interests of participating countries diverge. This is generic for any fixed subsidy rate policy, because once countries receive the maximum subsidy in their smaller groups, they gain no additional financial incentive from merging.

However, the considered progressive subsidy designs may reduce political resistance from smaller or less central countries, facilitate multilateral negotiations, and support robust, stable infrastructure planning aligned with long-term decarbonization goals. It will also encourage larger and more integrated coalitions, essential for transnational hydrogen corridors. This scheme promotes larger cooperation with the likelihood of reducing fragmented investments.

For simple allocation rules, it can be concluded that although the "Proportional to internal cost" allocation is satisfactory for all coalitions in most, but not all the cases. Perspectives include further development of the case study, sensitivity analysis, coupling of optimization tools, and refinement of subsidy scenarios.

Acknowledgement

The project is supported by the National Research, Development, and Innovation Fund of Hungary [grant numbers: OTKA FK 146575 and OTKA K 146649].

References

1. Lu, X., Ren, S., Cui, Y., Yin, X., Chen, X., Zhang, Y., Moghtaderi, B.: A novel site selection approach for Co-location of petrol-hydrogen fueling stations using a game theory-based multi-criteria decision-making model. Int. J. Hydrogen Energy. 106, 1443–1461 (2025). https://doi.org/10.1016/j.ijhydene.2025.02.076.
2. EHB: A European Hydrogen Infrastructure Vision Covering 28 Countries, https://ehb.eu/files/downloads/ehb-report-220428-17h00-interactive-1.pdf, last accessed 2025/07/14.
3. European Hydrogen Backbone: Implementation Roadmap - Cross Border Projects and Costs update, https://ehb.eu/files/downloads/EHB-2023-20-Nov-FINAL-design.pdf, last accessed 2025/07/26.
4. European Union: Regulation of the European Union Parliament and of the Council, https://eur-lex.europa.eu/legal-content/EN/TXT/?uri=celex%3A32022R0869, last accessed 2025/07/26.
5. EHB: Five hydrogen supply corridors for Europe in 2030, https://ehb.eu/files/downloads/EHB-Supply-corridor-presentation-Full-version.pdf, last accessed 2025/07/14.
6. SEEHyC: The South-East European Hydrogen Corridor (SEEHyC) initiative Project Description, https://www.seehyc.eu/project-description/, last accessed 2025/08/14.

QUBO formulations for minimizing breaks in sports timetabling

Levente Gegő and Viktória Nemkin

Department of Computer Science and Information Theory,
Budapest University of Technology and Economics
lgego@cs.bme.hu, nemkin@cs.bme.hu

Abstract. We study QUBO formulations for minimizing breaks in double round-robin tournaments, where each team plays every other team twice, once at home and once away. A break occurs when a team plays two consecutive home games or two consecutive away games. Minimizing breaks improves fairness, reduces uneven travel burdens and helps increase revenue.
We compare two single-phase QUBO formulations that determine both the timetable and the home-away assignment: one based on permutation-matrix encoding and another one based on sorting-network encoding. The sorting-network formulation has an asymptotically smaller problem graph with lower maximum vertex degree. For the tested problem sizes, however, it uses about ten times more vertices, and its edge count becomes smaller only for the larger instances in our range. Its main structural advantage is having substantially lower maximum vertex degree, which may become useful for minor embedding on future hardware.

Keywords: QUBO · sports timetabling · double round-robin tournaments · minimizing breaks.

1 Introduction

Scheduling sports leagues requires balancing fairness, attractiveness, venue availability, broadcaster requests, and other practical constraints. A comprehensive survey by Devriesere, Csató, and Goossens [4] identifies scheduling as one of the core components of tournament design, alongside format selection, seeding, draw, and ranking.

A widely used format is the *double round-robin tournament* (DRRT), in which every team plays every other team exactly twice, once at home and once away. We consider the minimization of *breaks*: a break occurs when a team plays two consecutive home games or two consecutive away games. Breaks are undesirable because they create unequal travel burdens and may decrease revenue. Early successful approaches used integer programming and constraint programming, often in multiple phases. Nemhauser and Trick [9] scheduled the 1997–98 Atlantic Coast Conference basketball league using a *first-break-then-schedule* decomposition. Trick [11] later proposed the reverse *first-schedule-then-break* model. Rasmussen and Trick [10] developed a hybrid IP/CP framework based on Benders

cuts, while Durán, Guajardo, and Sauré [5] used a single-phase IP formulation for the South American qualifiers of the 2018 FIFA World Cup.

More recently, Kuramata, Katsuki, and Nakata [8] studied break minimization with quantum annealing in the first-schedule-then-break setting: given a fixed timetable, they sought a home-away assignment that minimizes the number of breaks. Their method eliminates the feasibility constraints by substitution, so feasibility is built into the variables rather than imposed through penalties. They also relate embeddability to the maximum vertex degree of the problem graph: its maximum vertex degree is 4 for mirrored DRRTs (MDRRTs) and 8 for general DRRTs. Using the heuristic of Cai, Macready, and Roy [3], they reported successful embeddings on D-Wave Advantage 1 for MDRRT instances with up to 48 teams and for general DRRT instances with up to 28 teams. In their computational experiments, the annealer matched known optimal solutions for MDRRT instances with up to 20 teams and for DRRT instances with up to 12 teams.

In contrast, we formulate the full single-phase problem, deciding both the timetable and the home-away assignment within one QUBO. We give two such formulations: one based on the standard permutation-matrix encoding and one derived from the sorting-network permutation encoding of Friedl, Gegő, Kabódi, and Nemkin [6]. The problem graph of the latter is asymptotically smaller and has lower maximum vertex degree. In the tested range, however, the finite-size results are mixed: the sorting-network formulation uses roughly ten times more vertices, and it has fewer edges only once the number of teams exceeds 20. Its main structural advantage is having substantially lower maximum vertex degree, which may become useful for minor embedding on future hardware. On the currently available D-Wave Advantage 2, both formulations can be embedded only up to 4 teams.

2 Prerequisites

The *Quadratic Unconstrained Binary Optimization* (QUBO) problem asks to minimize a quadratic objective over binary variables,

$$\min_{x \in \{0,1\}^n} \sum_{i \le j} q_{i,j}\, x_i x_j,$$

and can be solved with quantum annealers. The corresponding *problem graph* has one vertex per variable x_i and an edge for each nonzero coefficient $q_{i,j}$, where $i \neq j$.

A *polynomial representation* of a Boolean function $f : \{0,1\}^k \to \{0,1\}$ is a non-negative multilinear polynomial $g : \mathbb{R}^{k+m} \to \mathbb{R}_{\ge 0}$, with auxiliary variables z, such that $\min_z g(x,z) = 0$ if and only if $f(x) = 1$. The representation is *uniform* if the number of minimizing z assignments is the same for every satisfying x. Higher-degree representations can be reduced to quadratic form by introducing additional auxiliary variables.

These representations are used as penalties to describe constraints: violating a constraint gives a positive contribution, while satisfying it gives zero. In the final QUBO, all such penalties are multiplied by a coefficient larger than the maximum possible objective value.

2.1 Permutation encoding via sorting networks

The standard encoding, called *permutation-matrix encoding*, represents a permutation π of $\{1, \ldots, n\}$ with n^2 binary indicator variables. The permutation condition is enforced by row and column sum constraints. When these are added as penalties, it yields a problem graph with maximum vertex degree $O(n)$.

Friedl, Gegő, Kabódi, and Nemkin [6] propose an encoding based on sorting networks [7]. These networks consist of *compare-exchange gates*. A gate takes two input numbers, outputs them in non-decreasing order, and has an associated comparison bit indicating whether the two inputs were swapped. The valid behavior of a gate is described by a penalty: its variables are the input bits, output bits, and comparison bit of the gate, and the penalty is zero exactly when these bits describe a possible state of the gate. A sorting-network is an oblivious sorting algorithm, meaning that the sequence of gates is fixed for a given input size. The gates are linked by sharing variables between consecutive gates: an output variable of a gate is the corresponding input variable of the next. Summing the gate penalties over the whole network gives a penalty that is zero exactly when the variable assignment describes a valid execution of the network.

Fixing the output variables of the network to the identity permutation forces the input variables to encode a permutation. With the AKS network of Ajtai, Komlós, and Szemerédi [1], the problem graph of this encoding has $O(n \log^2 n)$ vertices and maximum vertex degree $O(\log n)$ [6, Corollary 2]. In practice we use Batcher's odd-even merge-sort [2], incurring one extra $\log n$ factor on the number of vertices.

An involution is a self-inverse permutation and a derangement has no fixed points. These constraints can be added to the sorting-network encoding with the same asymptotic behaviour [6, Theorems 2–3].

3 Formulations

We present two QUBO formulations for a DRRT with n teams (assumed even) and $r = 2(n-1)$ rounds. Each round is an involutive derangement π, where $\pi(j)$ is the opponent of team j: if j plays k then k plays j, and no team plays itself. Each pair meets twice overall, once at home and once away. A *break* for team j occurs between rounds i and $(i+1)$ when j is at home in both or away in both. The objective is to minimize the total number of breaks.

3.1 Permutation-matrix encoding (PM)

We use the standard permutation-matrix encoding as a baseline.

Variables. For round $i \in \{0, \ldots, r-1\}$ and teams $j, k \in \{0, \ldots, n-1\}$ let

- $p_{i,j,k} \in \{0,1\}$: indicator that team j plays team k in round i,
- $ha_{i,j} \in \{0,1\}$: 0 if team j is at home, 1 if away in round i,
- $hap_{i,j,k} \in \{0,1\}$: auxiliary variable for the product $p_{i,j,k} \cdot ha_{i,j}$.

In the final QUBO, we substitute $p_{i,k,j} = p_{i,j,k}$ for all $j < k$ (involution) and $p_{i,j,j} = 0$ (derangement), which reduces the size of p.

Constraints. These are implemented as penalties added to the quadratic objective, each with coefficient $(M+1)$, where $M = n(2n-3)$ is the maximum possible number of breaks.

1. **One opponent per round.**
   For all i, j add $\left(\sum_{k \neq j} p_{i,j,k} - 1\right)^2$.
2. **Each pairing occurs exactly once at home and once away.**
   For all $j \neq k$, add $\left(\sum_i (p_{i,j,k} - hap_{i,j,k}) - 1\right)^2 + \left(\sum_i hap_{i,j,k} - 1\right)^2$.
3. **One home per game.**
   When teams j and k meet in round i, exactly one must be home. For all i and $j < k$, add $\left(hap_{i,j,k} + hap_{i,k,j} - p_{i,j,k}\right)^2$.
   When $p_{i,j,k} = 1$, this forces $hap_{i,j,k} + hap_{i,k,j} = 1$, i.e. $ha_{i,j} + ha_{i,k} = 1$. When $p_{i,j,k} = 0$, both *hap* variables are zero and the constraint is satisfied trivially.
4. **Setting the auxiliary product variables** $hap_{i,j,k} = p_{i,j,k} \cdot ha_{i,j}$**.**
   For each i, j, k, add $\Big(p_{i,j,k}\, ha_{i,j} - 2p_{i,j,k}\, hap_{i,j,k} - 2\, ha_{i,j}\, hap_{i,j,k} + 3\, hap_{i,j,k}\Big)$.

Objective. A break between rounds i and $(i+1)$ for team j contributes $(1 - ha_{i,j} - ha_{i+1,j} + 2\, ha_{i,j}\, ha_{i+1,j})$ to the objective (this equals 1 if and only if $ha_{i,j} = ha_{i+1,j}$). Summing over all j and $i \in \{0, \ldots, r-2\}$ gives the quadratic objective.

Problem graph. The problem graph of this formulation has $O(n^3)$ vertices and maximum vertex degree $O(n)$.

3.2 Sorting-network encoding (SN)

Variables. Let $b = \lceil \log_2 n \rceil$. For each round i and team j, let $x_{i,j} \in \{0,1\}^b$ be the binary encoding of j's opponent in round i, and $ha_{i,j} \in \{0,1\}$ as in PM.

Constraints. Instead of compare-exchange gates, we use controlled swap gates, which do not penalize swapping inputs that are already in the correct order. This significantly r educes t he n umber o f a uxiliary v ariables. W ith t his, w e sacrifice uniformity only: several control-bit assignments may realize the same permutation, but each gate penalty still enforces that the outputs are the same numbers as the inputs, either swapped or unchanged.

In both types of constraints below, the $x_{i,j}$ and $ha_{i,j}$ are carried together as a pair throughout the sorting network.

1. **Row constraints: involution and derangement.**
   For each round i, the map $j \mapsto x_{i,j}$ must be an involutive derangement, enforced as in Section 2.1. The involution and derangement penalties apply to the $x_{i,j}$ only. The constraint that exactly one of the two opponents in each game is at home is enforced in the network: the team at input position k and the team at output position k are opponents, so we constrain their ha variables to sum to 1.
2. **Column constraints: balanced home-away schedule.**
   For each team j, the pairs $(ha_{i,j}, x_{i,j})$ over all rounds must form a permutation of $\{0,1\} \times (\{0,\ldots,n-1\} \setminus \{j\})$, encoded as $(b+1)$-bit values, ensuring every opponent is met once at home and once away.

All penalties are multiplied by $(M+1)$, as in the PM formulation. Within the row and column constraint penalties, the largest internal coefficient is of size $O(\log^2 n)$, which arises from the T_1 threshold-penalty construction of [6] used for the derangement constraints.

Objective. The break objective is identical to that of the PM formulation.

Problem graph. Using Batcher's odd-even merge-sort [2], the problem graph of this formulation has $O(n^2 \log^3 n)$ vertices and maximum vertex degree $O(\log n)$.

4 Results

We generated both QUBOs and measured vertex and edge counts of the problem graphs (Figure 1). PM uses roughly ten times fewer vertices for the tested sizes, while SN has fewer edges only for $n > 20$.

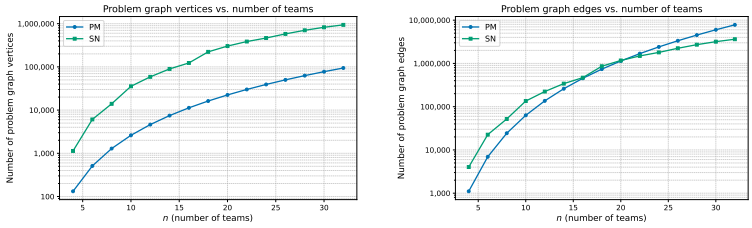

Fig. 1. Problem graph vertex count (left) and edge count (right) versus number of teams n, on a logarithmic scale.

Both formulations solve the full single-phase problem. Feasibility is enforced by QUBO penalties, which create a large problem graph and large coefficients.

This limitation is absent from Kuramata et al. [8], where the timetable is fixed and only the home-away assignment is optimized. Their constraint-free QUBO could be embedded on D-Wave Advantage 1 up to 48 teams for MDRRTs and 28 teams for general DRRTs using the heuristic method of Cai, Macready, and Roy [3]. Our larger QUBOs are much harder to embed: without direct D-Wave access, we ran only the classical embedding step using [3] against the D-Wave Advantage 2 topology, without performing actual annealing, and obtained embeddings only up to 4 teams in both formulations.

Thus neither formulation is currently practical for quantum annealing at realistic league sizes. Still, the low maximum vertex degree of SN is promising. Kuramata et al. attribute the better MDRRT embeddability partly to the lower maximum vertex degree of the problem graph. In our experiments SN likewise has substantially lower maximum vertex degree than PM (see the Appendix), suggesting that sparse permutation encodings may become useful with future hardware.

Acknowledgements

Author Viktória Nemkin was supported by the Doctoral Excellence Fellowship Programme (DCEP), funded by the National Research, Development and Innovation Fund of the Ministry of Culture and Innovation and the Budapest University of Technology and Economics.

References

1. Ajtai, M., Komlós, J., Szemerédi, E.: Sorting in $c \log n$ parallel steps. Combinatorica **3**(1), 1–19 (1983)
2. Batcher, K.E.: Sorting networks and their applications. In: Proceedings of the AFIPS Spring Joint Computer Conference, vol. 32, pp. 307–314. ACM (1968)
3. Cai, J., Macready, W.G., Roy, A.: A practical heuristic for finding graph minors. arXiv preprint arXiv:1406.2741 (2014)
4. Devriesere, K., Csató, L., Goossens, D.: Tournament design: A review from an operational research perspective. European Journal of Operational Research **324**(1), 1–21 (2025)
5. Durán, G., Guajardo, M., Sauré, D.: Scheduling the South American qualifiers to the 2018 FIFA World Cup by integer programming. European Journal of Operational Research **262**(3), 1109–1115 (2017)
6. Friedl, K., Gegő, L., Kabódi, L., Nemkin, V.: Succinct QUBO formulations for permutation problems by sorting networks. arXiv preprint arXiv:2603.07579 (2026)
7. Knuth, D.E.: Networks for Sorting. In: The Art of Computer Programming, Vol. 3: Sorting and Searching, chap. 5.3.4, pp. 219–234. Addison-Wesley, 2nd edn. (1998)
8. Kuramata, M., Katsuki, R., Nakata, K.: Solving large break minimization problems in a mirrored double round-robin tournament using quantum annealing. PLOS ONE **17**(4), e0266846 (2022)
9. Nemhauser, G.L., Trick, M.A.: Scheduling a major college basketball conference. Operations Research **46**(1), 1–8 (1998)

10. Rasmussen, R.V., Trick, M.A.: A Benders approach for the constrained minimum break problem. European Journal of Operational Research **177**(1), 198–213 (2007)
11. Trick, M.A.: A schedule-then-break approach to sports timetabling. In: Burke, E., Erben, W. (eds.) Practice and Theory of Automated Timetabling III. LNCS, vol. 2079, pp. 242–253. Springer (2001)

Appendix: Degree Distribution Tables

Table 1. Degree distributions of the problem graphs for PM and SN: number of vertices of each degree, for $n \in \{4, 10, 16, 20, 26, 30\}$.

	PM						SN					
degree	4	10	16	20	26	30	4	10	16	20	26	30
2	–	–	–	–	–	–	72	1088	3200	7740	13488	18200
3	–	–	–	–	–	–	144	1784	4160	5040	8124	10580
4	–	–	–	–	–	–	372	15104	54320	137416	265364	378740
5	–	–	–	–	–	–	168	2340	6240	12160	20800	27840
6	–	–	–	–	–	–	228	12936	48240	126636	246676	353580
7	8	–	–	–	–	–	–	–	–	–	–	–
8	16	–	–	–	–	–	–	–	–	–	–	–
10	–	–	–	–	–	–	56	20	32	40	52	60
11	–	–	–	–	–	–	16	160	448	720	1248	1680
12	–	–	–	–	–	–	48	–	–	–	–	–
13	72	–	–	–	–	–	–	720	1920	–	–	–
15	–	–	–	–	–	–	–	–	–	3800	6500	8700
16	–	–	–	–	–	–	12	–	–	–	–	–
19	–	20	–	–	–	–	–	–	–	–	–	–
20	–	160	–	–	–	–	18	840	2880	–	–	–
23	36	–	–	–	–	–	–	–	–	–	–	–
24	–	–	–	–	–	–	–	–	–	5480	10348	14820
28	–	–	–	–	–	–	–	90	240	–	–	–
31	–	–	32	–	–	–	–	–	–	–	–	–
32	–	–	448	–	–	–	–	–	–	–	–	–
34	–	–	–	–	–	–	–	–	–	304	500	812
36	–	–	–	–	–	–	–	432	1560	–	–	–
37	–	1620	–	–	–	–	–	–	–	–	–	–
39	–	–	–	40	–	–	–	–	–	152	300	116
40	–	–	–	720	–	–	–	–	–	–	–	–
44	–	–	–	–	–	–	–	–	–	3382	6600	9512
51	–	–	–	–	52	–	–	–	–	–	–	–
52	–	–	–	–	1248	–	–	–	–	–	–	–
59	–	–	–	–	–	60	–	–	–	–	–	–
60	–	–	–	–	–	1680	–	–	–	–	–	–
61	–	–	7200	–	–	–	–	–	–	–	–	–
71	–	810	–	–	–	–	–	–	–	–	–	–
77	–	–	–	14440	–	–	–	–	–	–	–	–
101	–	–	–	–	32500	–	–	–	–	–	–	–
117	–	–	–	–	–	50460	–	–	–	–	–	–
119	–	–	3600	–	–	–	–	–	–	–	–	–
151	–	–	–	7220	–	–	–	–	–	–	–	–
199	–	–	–	–	16250	–	–	–	–	–	–	–
231	–	–	–	–	–	25230	–	–	–	–	–	–

Global convergence of scaled Polyak subgradient method for robust phase retrieval

Morteza Rahimi and Masoud Ahookhosh

Department of Mathematics, University of Antwerp, Middelheimlaan 1, B-2020 Antwerp, Belgium
morteza.rahimi@uantwerpen.be, masoud.ahookhosh@uantwerpen.be

Abstract. This study is devoted to the class of weakly convex functions satisfying quadratic growth condition. The convergence analysis of the subgradient algorithm with scaled Polyak's step-size to global minima for this class of functions is studied. The preliminary numerical experiments on the robust phase retrieval problem indicate promising behavior for the method, validating our theoretical foundations.

Keywords: Weakly convex optimization · Scaled Polyak subgradient algorithm · Quadratic growth condition · Robust phase retrieval problem.

1 Introduction

This paper addresses the nonsmooth and nonconvex optimization problem

$$\min_{x \in X} f(x), \tag{1}$$

where $f : \mathbb{R}^m \to \overline{\mathbb{R}}$ is a proper, possibly nonsmooth and nonconvex function, and $X \subseteq \mathrm{dom}(f)$ is nonempty, closed, and convex. We assume that the optimal solution set $\mathcal{X}^*$ is nonempty and that the optimal value f^* is finite. In contrast to convex settings, such problems are significantly more challenging due to the lack of smoothness, the presence of intricate nonconvex landscapes with multiple critical points, and the fact that local minimizers need not be global. Moreover, many existing methods require initialization sufficiently close to the solution set to guarantee convergence.

To address problem (1), first-order methods, particularly subgradient methods, are widely employed due to their simplicity, low memory requirements, and reliance solely on function values and subgradients [8]. Despite their practical success in large-scale applications such as signal processing and machine learning [6,10], their theoretical guarantees in the nonconvex setting remain limited. Existing results typically rely either on restrictive assumptions on the objective (e.g., smoothness) or on carefully tuned diminishing step-sizes, often leading to slow convergence and sensitivity to initialization. In particular, convergence is frequently guaranteed only when the initial point lies sufficiently close to the solution set, limiting practical applicability [4,9].

1.1 Motivation

In this work, we focus on the broad and practically significant class of weakly convex functions. A function $h : \mathbb{R}^m \to \overline{\mathbb{R}}$ is said to be ρ-weakly convex on a convex set $S \subseteq \mathrm{dom}(h)$ if the perturbed function $x \mapsto h(x) + \frac{\rho}{2}\|x\|^2$ is convex for some constant $\rho \geq 0$. Equivalently, this implies that

$$h(y) \geq h(x) + \langle \zeta, y - x \rangle - \frac{\rho}{2}\|y - x\|^2, \qquad \forall x, y \in \mathbb{R}^n, \quad \forall \zeta \in \partial h(x). \tag{2}$$

Weak convexity effortlessly captures many nonsmooth composite problems common in modern data science. However, in the seminal work studying subgradient methods for sharp weakly convex functions [4], the linear convergence is guaranteed only if the algorithm is initialized within a "tube" or basin of attraction strictly close to the optimal set $\mathcal{X}^*$. Hence, the primary motivation of our research is to overcome this limitation by developing a subgradient-based method that is intrinsically free from the burden of local initialization. Here, we aim at establishing the global convergence for random starting points.

We here assume that the objective function f admits a *quadratic growth* (QG) condition, i.e., there exists $\mu > 0$ on X such that

$$f(x) - f^* \geq \mu \, \mathrm{dist}^2(x, \mathcal{X}^*), \qquad \forall x \in X.$$

The QG condition is a natural relaxation of the sharpness error bound (which relies on a purely linear residual) and provides a more realistic geometric landscape for many non-convex inverse problems [7].

Motivating example. A quintessential example that motivates our framework is the phase retrieval problem, which seeks to reconstruct a signal from phaseless quadratic measurements. This problem appears in real-world applications in various fields like speech processing, and imaging. Given the vectors $\{a_i\}_{i=1}^m \subseteq \mathbb{R}^n$ and $b \in \mathbb{R}^m$, the real-valued version of the problem concentrates on finding a solution x which satisfies the magnitude conditions $\langle a_i, x \rangle^2 \approx b_i$ for all $i = 1, 2, \ldots, m$. In this situation, the problem can be formulated as [5]:

$$\min_x \tfrac{1}{m} \sum_{i=1}^m |\langle a_i, x \rangle^2 - b_i|. \tag{3}$$

Invoking [9, Proposition 3.11], this function is weakly convex. Furthermore, it has been shown in the literature that such formulations naturally satisfy the QG condition once a sufficient number of measurements are collected [1].

1.2 Notations

In this paper, the standard inner product and Euclidean norm in $\mathbb{R}^n$ are denoted by $\langle \cdot, \cdot \rangle$ and $\|\cdot\| := \sqrt{\langle \cdot, \cdot \rangle}$, respectively. The *interior* of a nonempty set $S \subseteq \mathbb{R}^n$ is indicated by $\mathrm{int}\, S$. The distance and the projection of a point $x \in \mathbb{R}^n$ onto S is defined by $\mathrm{dist}(x; S) := \inf_{z \in S} \|x - z\|$ and $\mathrm{proj}_S(x) := \mathrm{argmin}_{z \in S} \|x - z\|$, respectively. The indicator function of S, denoted by δ_S, is defined by $\delta_S(x) = 0$ if $x \in S$ and $\delta_S(x) = +\infty$ otherwise. A function $h : \mathbb{R}^n \to \mathbb{R} := \mathbb{R} \cup \{+\infty\}$

is said to be proper if its effective domain $\mathrm{dom}(h) := \{x \in \mathbb{R}^n : h(x) < +\infty\}$ is nonempty. Let $h : \mathbb{R}^n \to \overline{\mathbb{R}}$ be a proper function that is locally Lipschitz at $\bar{x} \in \mathrm{int}\,\mathrm{dom}(h)$. The *Clarke's subdifferential* of h at $\bar{x}$ [3] is defined as $\partial h(\bar{x}) := \{\zeta \in \mathbb{R}^n : \langle \zeta, d\rangle \leq h^\circ(\bar{x}; d),\ \forall d \in \mathbb{R}^n\}$ where $h^\circ(\bar{x}; d) := \limsup_{\substack{x \to \bar{x} \\ t \downarrow 0}} \frac{h(x+td)-h(x)}{t}$.

2 Scaled Polyak subgradient method

In this section, we first establish the convergence analysis of the scaled Polyak subgradient method for the nonsmooth and constrained weakly convex optimization problems of the form (1). We begin with the following assumption.

Assumption I *We assume that the following properties hold:*

1. *The function f is ρ-weakly convex with $\rho > 0$ on a open convex set $X' \supseteq X$;*
2. *The function f admits the QG condition on X with constant $\mu > \rho$.*

A point $x \in X$ is said to be a *stationary* point of (1) if $0 \in \partial(f + \delta_X)(x)$. The following lemma shows that the stationary points are optimal.

Lemma 1. *The stationary points of* (1) *are optimal solutions.*

Proof. By indirect proof, let $x \in X \setminus \mathcal{X}^*$ be a stationary point of (1), i.e., $0 \in \partial(f+\delta_X)(x)$. Let $x^* \in \mathrm{proj}_{\mathcal{X}^*}(x)$. Then, applying (2) together with the QG condition, we come to

$$\mu\,\mathrm{dist}^2(x; \mathcal{X}^*) \leq f(x) - f(x^*) \leq \rho\|x - x^*\|^2 = \rho\,\mathrm{dist}^2(x; \mathcal{X}^*),$$

leading to a contradiction, since $\mu > \rho$. □

In the following we present the scaled Polyak subgradient algorithm.

Algorithm 1: SPSG (Scaled Polyak SubGradient Algorithm)

Input: $x_0 \in X$; $\sigma > 0$.
begin
  while *the stopping criteria do not hold* **do**
    Choose $\zeta_k \in \partial f(x_k)$ and set $\widehat{x}_{k+1} = x_k - \frac{f(x_k)-f^*}{\sigma\|\zeta_k\|^2}\zeta_k$;
    Set $x_{k+1} = \mathrm{proj}_X(\widehat{x}_{k+1})$ and $k = k + 1$;
  end
  $x_{best} := x_k$
end
Output: x_{best}.

Although this approach requires knowing the optimal value of the problem (1), this requirement is reasonable in certain scenarios, such as when employing the exact penalty method to solve nonlinear equations. We next analyze the convergence of the sequence generated by Algorithm 1.

Theorem 1 (Global convergence of SPSG). *Let $\{x_k\}_{k\geq 0}$ be generated by SPSG with the scaled parameter $\sigma > \frac{\mu}{2(\mu-\rho)}$. Then, the following assertions hold:*

(a) For $q_k := 1 - \frac{\big(2\sigma(\mu-\rho)-\mu\big)}{L^2\sigma^2}\mu\,\mathrm{dist}^2(x_k;\mathcal{X}^*)$ *and* $L := \sup_k \|\zeta_k\|$*, one has*

$$\mathrm{dist}^2(x_{k+1};\mathcal{X}^*) \le q_k\,\mathrm{dist}^2(x_k;\mathcal{X}^*); \tag{4}$$

(b) If $L<\infty$*, then* $\lim_{k\to\infty} f(x_k) = f^*$ *and* $\lim_{k\to\infty}\mathrm{dist}(x_k;\mathcal{X}^*) = 0$*;*
(c) We have $f_k^* - f^* \le \frac{\sigma L\,\mathrm{dist}(x_0;\mathcal{X}^*)}{\sqrt{2\sigma(1-\rho/\mu)-1}\sqrt{k+1}}$*, for each* $k\ge 0$*.*

Proof. (a) If $x_k\in\mathcal{X}^*$, then $f(x_k)=f^*$ and $\mathrm{dist}(x_k;\mathcal{X}^*)=0$. Moreover, we have $x_{k+1}=\mathrm{proj}_X(x_k)=x_k$, and (4) holds. Let us examine the case that $x_k\notin\mathcal{X}^*$. We choose $x^*\in\mathrm{proj}_{\mathcal{X}^*}(x_k)$. Using (2) and QG condition we obtain

$$\langle\zeta_k, x^*-x_k\rangle \le f^* - f(x_k) + \rho\|x_k-x^*\|^2 \le (\rho/\mu-1)\big(f(x_k)-f^*\big).$$

This together with the nonexpansiveness of the projection operator gives us

$$\begin{aligned}
\mathrm{dist}^2(x_{k+1};\mathcal{X}^*) &\le \|x_{k+1}-x^*\|^2 \le \big\|(x_k-x^*) - \tfrac{f(x_k)-f^*}{\sigma\|\zeta_k\|^2}\zeta_k\big\|^2\\
&\le \mathrm{dist}^2(x_k;\mathcal{X}^*) - \frac{2(1-\rho/\mu)\big(f(x_k)-f^*\big)^2}{\sigma\|\zeta_k\|^2} + \frac{\big(f(x_k)-f^*\big)^2}{\sigma^2\|\zeta_k\|^2}\\
&\le \mathrm{dist}^2(x_k;\mathcal{X}^*) - \frac{\big(f(x_k)-f^*\big)^2}{\sigma^2L^2}\big(2\sigma(1-\rho/\mu)-1\big), \qquad (5)\\
&\le \mathrm{dist}^2(x_k;\mathcal{X}^*) - \frac{\mu^2\,\mathrm{dist}^4(x_k;\mathcal{X}^*)}{\sigma^2L^2}\big(2\sigma(1-\rho/\mu)-1\big),
\end{aligned}$$

verifying (4). (b) Let $L<\infty$. Summing inequality (5) from $k=0$ to N yields

$$\tfrac{1}{\sigma^2L^2}\big(2\sigma(1-\rho/\mu)-1\big)\sum_{k=0}^{N}\big(f(x_k)-f^*\big)^2 \le \mathrm{dist}^2(x_0;\mathcal{X}^*) < \infty, \tag{6}$$

ensuring $\lim_{k\to\infty} f(x_k)=f^*$. Moreover, $\lim_{k\to\infty}\mathrm{dist}(x_k;\mathcal{X}^*)=0$ by QG condition. (c) It is derived from (6). This completes the proof. □

2.1 Application to robust phase retrieval

Here, we evaluate the empirical performance of the SPSG[1] with $\sigma=1$. To ensure a rigorous assessment, we focus on a noise-free phase retrieval configuration. Let $n=5000$ denote the signal dimension and m represent the number of measurements, where the sampling complexity is characterized by the ratio $\alpha=m/n\in\{3.0,3.5,4.0,4.5,5.0\}$. Regarding to the experimental setup, the measurement vectors $\{a_i\}_{i=1}^m$ are drawn from a standard Gaussian distribution $\mathcal{N}(0,I_n)$ and subsequently normalized to unit ℓ_2-norm to ensure numerical stability. The ground-truth signal $x^*\in\mathbb{R}^n$ is sampled from $\mathcal{N}(0,I_n)$ and scaled such that $\|x^*\|=1$. Consistent with (3), the phaseless observations are generated via $b_i=|\langle a_i,x^*\rangle|^2$. Unless otherwise specified, we employ a random initialization $x_0\sim\mathcal{N}(0,I_n)$ to test the algorithm's global convergence capability.

[1] github.com/Morteza-Rahimi68/SPSG-for-robust-phase-retrieval.git

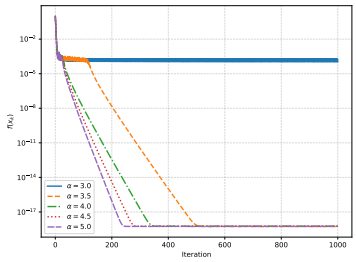

(a) Loss function values.

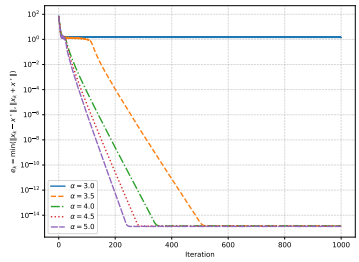

(b) Evolution of reconstruction error e_k.

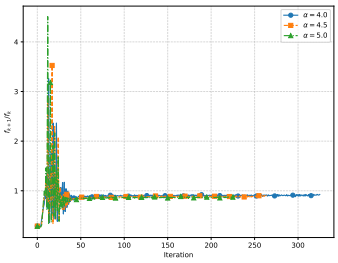

(c) Empirical linear ratios of loss value.

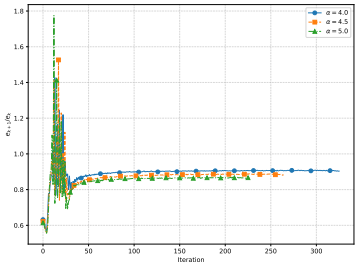

(d) Empirical linear ratios of error.

Fig. 1: Performance of SPSG for $n = 5000$ and various sampling ratios α.

The convergence characteristics of the SPSG are depicted in Figure 1. For $\alpha \geq 3.5$, the algorithm successfully recovers the signal to machine precision (10^{-15}), even with a completely random initialization. Notably, the duration of the initial "plateau" phase, where the iterates navigate the non-convex landscape to find a descent direction, decreases as the sampling ratio α increases. The results confirm that even with a completely random initialization, the PSSPGA effectively navigates the non-smooth L_1 loss surface, demonstrating its robustness against the lack of a spectral starting point.

To further investigate the behavior of local convergence, the empirical ratios f_{k+1}/f_k and e_{k+1}/e_k are illustrated in Figures 1(c) and 1(d), respectively. Following an initial transient search phase (approximately first 50 iterations), the ratios for all successful cases stabilize at a constant value strictly less than unity (approximately between 0.85 and 0.92). This stabilization provides strong empirical evidence of linear convergence (also known as geometric convergence) once the iterates enter the basin of attraction of the global minimizer. The consistency of these ratios highlights the robustness of the SPSG in maintaining a steady descent rate without manual parameter tuning.

To evaluate the sample efficiency of the SPSG, we conduct a phase transition study by varying the sampling ratio $\alpha = m/n$ with $n = 1000$. We stop after maximum 1000 iterations and a success tolerance of 10^{-6}, with each data point representing the average success rate over 20 independent trials. To test the global convergence of the algorithm, we employ a random initialization $x_0 \sim \mathcal{N}(0, I_n)$.

As illustrated in Figure 2, the algorithm exhibits a sharp phase transition from failure to success. Although the success rate is zero for $\alpha < 2.8$, it increases abruptly and achieves empirical success 100 at $\alpha \approx 3.8$. This result is particularly significant when compared to the well-known theoretical benchmark of $m \geq 4n$ often cited in the literature [2]. The fact that SPSG reaches a stable success regime slightly before the $4n$ threshold, even with random initialization and a non-smooth loss function, demonstrates its exceptional sample efficiency and robustness.

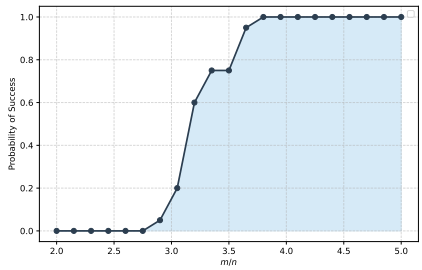

Fig. 2: Empirical success rate versus sampling ratio $\alpha = {}^{m}/_{n}$ ($n = 1000$) averaged over 20 trials.

References

1. Bandeira, A. S., Cahill, J., Mixon, D. G., Nelson, A. A.: Saving phase: Injectivity and stability for phase retrieval. Applied and Computational Harmonic Analysis **37**(1), 106-125 (2014)
2. Candes, E. J., Li, X., Soltanolkotabi, M.: Phase retrieval via Wirtinger flow: Theory and algorithms. IEEE Transactions on Information Theory **61**(4), 1985-2007 (2015)
3. Clarke, F.H.: Optimization and Nonsmooth Analysis. SIAM, (1990)
4. Davis, D., Drusvyatskiy, D., MacPhee, K. J., Paquette, C.: Subgradient methods for sharp weakly convex functions. Journal of Optimization Theory and Applications **179**(3), 962-982 (2018)
5. Davis, D., Drusvyatskiy, D., Paquette, C.: The nonsmooth landscape of phase retrieval. IMA Journal of Numerical Analysis **40**(4), 2652-2695 (2020)
6. Jain, P., Kar, P., et al.: Non-convex optimization for machine learning. Foundations and Trends® in Machine Learning **10**(3-4), 142-363 (2017)
7. Liao, F. Y., Ding, L., Zheng, Y.: Error bounds, PL condition, and quadratic growth for weakly convex functions, and linear convergences of proximal point methods. Journal of Global Optimization **94**, 235-263 (2026)
8. Nesterov, Y.: Lectures on Convex Optimization. Berlin: Springer International Publishing **173**, (2018)
9. Rahimi, M., Ghaderi, S., Moreau, Y., Ahookhosh, M: Projected subgradient methods for paraconvex optimization: Application to robust low-rank matrix recovery. arXiv preprint arXiv:2501.00427, (2025)
10. Wen, F., Chu, L., Liu, P., Qiu, R.C.: A survey on nonconvex regularization-based sparse and low-rank recovery in signal processing, statistics, and machine learning. IEEE Access **6**, 69883-69906 (2018)

On Bregman–Moreau Envelope Reformulations of DC Programs

Moslem Zamani, Morteza Rahimi, and Masoud Ahookhosh

Department of Mathematics, University of Antwerp, Antwerp, Belgium
moslem.zamani@uantwerpen.be, morteza.rahimi@uantwerpen.be, masoud.ahookhosh@uantwerpen.be

Abstract. In this paper, we investigate difference-of-convex (DC) problems. Our approach is based on the use of Bregman–Moreau envelopes, which provide a smooth surrogate framework for handling nonsmooth structures. We introduce and study both left and right Bregman–Moreau envelope formulations of DC functions. We provide a comprehensive theoretical analysis of the relationship between the original DC problem and its envelope counterparts. In particular, we show that the original problem and its envelope counterparts share the same optimal value. Moreover, we establish that stationary points of the envelope formulations correspond to critical points of the original DC problem. We also investigate the relationship between local minimizers of the original and envelope problems.

Keywords: Difference-of-convex problems · Bregman–Moreau Envelope · Smoothing techniques.

1 Introduction

In this paper, we consider the general difference-of-convex (DC) optimization problem,

$$\inf_{x\in\mathbb{R}^n} f(x) = p(x) - q(x), \tag{1}$$

where $f : \mathbb{R}^n \to \overline{\mathbb{R}}$ is a proper closed function and $p, q : \mathbb{R}^n \to \overline{\mathbb{R}}$ are proper closed convex functions. Throughout the paper, we assume the infimum in (1) is finite and $\infty - \infty = \infty$.

DC optimization problems arise naturally in a wide variety of applications, including in image processing [7] and supervised data classification [1], among others. This broad applicability is not surprising, as several important classes of nonconvex functions admit a DC decomposition. For example, any twice continuously differentiable function defined on a convex subset of $\mathbb{R}^n$ [4], as well as continuous piecewise linear functions [8], can be expressed as DC functions.

Smoothing techniques based on the Moreau envelope have been proposed to construct Lipschitz continuously differentiable DC approximations of a given DC function, thereby alleviating the difficulties arising from nonsmoothness

while preserving the underlying DC structure; see, e.g., [10,11]. These smoothed approximations can then be effectively combined with first-order optimization methods to solve DC programs (1). Such approaches have been shown to lead to efficient and numerically stable algorithms, which are particularly well-suited for large-scale nonsmooth optimization problems [10].

The Bregman–Moreau envelope is a natural generalization of the classical Moreau envelope obtained by replacing the squared Euclidean distance with a Bregman divergence. This construction inherits several favorable properties, such as smoothing effects and improved regularity, while preserving key structural features of the original function. In contrast to the classical Moreau envelope, the Bregman–Moreau envelope allows for greater flexibility through the choice of the kernel function, making it particularly well-suited for problems with non-Euclidean geometry. It has found important applications in optimization, especially in first-order methods, mirror descent schemes, and algorithms for nonsmooth and large-scale problems.

This paper is organized as follows. In Section 2, we recall basic notions from convex analysis and Bregman geometry. In Section 3, we study the left and right Bregman–Moreau envelope formulations of DC problem and establish their fundamental properties.

2 Preliminaries

Throughout the paper, $\|\cdot\|$ and $\langle\cdot,\cdot\rangle$ denote the Euclidean norm and the standard inner product on $\mathbb{R}^n$, respectively. For a set $X \subseteq \mathbb{R}^n$, we denote its convex hull by $\mathrm{co}(X)$. A function $\varphi : \mathbb{R}^n \to \overline{\mathbb{R}} = \mathbb{R} \cup \{+\infty\}$ is called *proper* if its effective domain $\mathrm{dom}(\varphi) := \{x \in \mathbb{R}^n \mid \varphi(x) < \infty\}$ is nonempty. It is called *closed* if its epigraph is a closed set. Moreover, the convex conjugate of g is defined by $\varphi^*(v) := \sup_{x\in\mathbb{R}^n}\{\langle v, x\rangle - \varphi(x)\}$. The (convex) subdifferential of φ at $x \in \mathrm{dom}\,\varphi$ is given by

$$\partial\varphi(x) := \{v \in \mathbb{R}^n \mid \varphi(y) \geq \varphi(x) + \langle v, y - x\rangle,\ \forall y \in \mathbb{R}^n\}.$$

Let $h : \mathbb{R}^n \to \overline{\mathbb{R}}$ be a proper, lower semicontinuous, and convex function, and let h be differentiable on $\mathrm{int}\,\mathrm{dom}(h) \neq \emptyset$. The function h is called *essentially smooth* if $\|\nabla h(x_k)\| \to \infty$ for every sequence $(x_k) \subset \mathrm{int}\,\mathrm{dom}(h)$ converging to a boundary point of $\mathrm{dom}(h)$. Moreover, it is said to be *essentially strictly convex* if it is strictly convex on every convex subset of $\mathrm{dom}(\partial h)$. If the function h satisfies the above properties it is said to be a Legendre function. These conditions imply that ∇h is continuous on $\mathrm{int}\,\mathrm{dom}(h)$; see, e.g., [9, Corollary 25.5.1].

Let h be a Legendre function. The associated *Bregman distance* $\mathrm{D}_h : \mathbb{R}^n \times \mathbb{R}^n \to \overline{\mathbb{R}}$ is defined by

$$\mathrm{D}_h(x, y) := \begin{cases} h(x) - h(y) - \langle\nabla h(y), x - y\rangle, & \text{if } y \in \mathrm{int}(\mathrm{dom}\, h), \\ +\infty, & \text{otherwise.} \end{cases}$$

Let $\gamma > 0$. The *(left) Bregman–Moreau envelope* and *proximity operator* of a function $\varphi : \mathbb{R}^n \to \overline{\mathbb{R}}$ are $\varphi_\gamma : \mathbb{R}^n \to \overline{\mathbb{R}}$ and $\operatorname{prox}^h_{\gamma\varphi} : \operatorname{int}\operatorname{dom}(h) \to \operatorname{int}\operatorname{dom}(h)$, respectively, defined as

$$\varphi^h_\gamma(y) = \inf_{x\in\mathbb{R}^n} \big\{\varphi(x) + \tfrac{1}{\gamma}\,\mathrm{D}_h(x,y)\big\}, \qquad \operatorname{prox}^h_{\gamma\varphi}(y) = \operatorname*{arg\,min}_{x\in\mathbb{R}^n} \big\{\varphi(x) + \tfrac{1}{\gamma}\,\mathrm{D}_h(x,y)\big\}.$$

By [2, Proposition 2.2], $\operatorname{dom}(\varphi^h_\gamma) = \operatorname{int}\operatorname{dom}(h)$. Additionally, $(\nabla h)^{-1} = \nabla h^*$ due to [9, Theorem 26.5]. Assuming $\operatorname{dom}(\varphi) \cap \operatorname{int}\operatorname{dom}(h) \neq \emptyset$, the Bregman–Moreau envelope can be expressed as:

$$\gamma\varphi^h_\gamma = \big(h^* - (\gamma h + \gamma f)^*\big) \circ \nabla h, \tag{2}$$

where $\circ$ denotes function composition; see [2, Proposition 2.4].

Fact 1 ([3, Propositions 3.5, 3.10, and 3.12]) *Let the Legendre function h be twice continuously differentiable on $\operatorname{int}\operatorname{dom}(h)$, let the function D_h be jointly convex on $\mathbb{R}^n \times \mathbb{R}^n$, and let the functions $\varphi(\cdot) + \mathrm{D}_h(\cdot, y)$ be coercive for every $y \in \operatorname{int}\operatorname{dom}(h)$. Then, the following assertions hold:*

(a) The proximity operator $\operatorname{prox}^h_{\gamma\varphi}$ is well-defined function;
(b) $\varphi^h_\gamma = (\nabla h + \gamma\partial\varphi)^{-1} \circ \nabla h$ and $\nabla\varphi^h_\gamma(x) = \frac{1}{\gamma}\nabla^2 h(x)\big(x - \operatorname{prox}^h_{\gamma\varphi}(x)\big)$;
(c) $y = \varphi^h_\gamma(x)$ if and only if $0 \in \gamma\partial\varphi(y) + \nabla^2 h(y)(y - x)$;
(d) $\widehat{x} = \operatorname{prox}^h_{\gamma\varphi}(x)$ if and only if $-\frac{1}{\gamma}(\nabla h(\widehat{x}) - \nabla h(x)) \in \partial\varphi(\widehat{x})$.

In this paper, we focus on the left Bregman–Moreau envelope; however, all results extend to the right envelope defined as $x \mapsto \inf_{y\in\mathbb{R}^n}\{\varphi(y) + \frac{1}{\gamma}\,\mathrm{D}_h(x,y)\}$.

3 Bregman–Moreau Envelope for DC problem

In this section, we study the following Bregman–Moreau envelope reformulation of DC problem (1):

$$\inf_{x\in\mathbb{R}^n} \big\{p^h_\gamma(x) - q^h_\gamma(x)\big\}. \tag{3}$$

It is known from [5] that the DC problem (1) and its associated Moreau envelope share the same optimal value. However, in the Bregman setting, this equivalence may fail without additional assumptions. To address this issue, we assume throughout the paper that $\operatorname{dom}(p), \operatorname{dom}(q) \subseteq \operatorname{int}\operatorname{dom}(h)$.

The following proposition shows that the equivalence extends to the Bregman–Moreau envelope. Before presenting the result, we recall Toland's Duality Theorem. According to John Toland's duality result [12], we have

$$\inf_{x\in\mathbb{R}^n} \big\{p(x) - q(x)\big\} = \inf_{v\in\mathbb{R}^n} \big\{q^*(v) - p^*(v)\big\}. \tag{4}$$

Proposition 1. *Problems* (1) *and* (3) *have the same optimal value.*

Proof. Using (2), we obtain

$$\begin{aligned}\inf_{x\in\mathbb{R}^n}\big\{p^h_\gamma(x)-q^h_\gamma(x)\big\} &= \tfrac{1}{\gamma}\inf_{x\in\mathbb{R}^n}\big\{\,(h^*-(h+\gamma p)^*)\circ\nabla h(x)-(h^*-(h+\gamma q)^*)\circ\nabla h(x)\big\}\\ &= \tfrac{1}{\gamma}\inf_{v\in\mathbb{R}^n}\big\{(h+\gamma q)^*(v)-(h+\gamma p)^*(v)\big\}\\ &= \tfrac{1}{\gamma}\inf_{x\in\mathbb{R}^n}\big\{h(x)+\gamma p(x)-(h(x)+\gamma q(x))\,\big\}=\inf_{x\in\mathbb{R}^n}\big\{p(x)-q(x)\big\},\end{aligned}$$

where in the third equality we apply (4) together with $\operatorname{dom}(p),\operatorname{dom}(q)\subseteq\operatorname{int}\operatorname{dom}(h)$. This justifies the result. □

We next adopt the following standing assumption, which is standard in the literature and ensures the required regularity properties; see, e.g., [2].

Assumption I

1. *The Legendre function h is twice continuously differentiable on* $\operatorname{int}\operatorname{dom}(h)$*;*
2. *The function* D_h *is jointly convex on* $\mathbb{R}^n\times\mathbb{R}^n$*;*
3. *For every* $y\in\operatorname{int}\operatorname{dom}h$*, the functions* $p(\cdot)+\mathrm{D}_h(\cdot,y)$ *and* $q(\cdot)+\mathrm{D}_h(\cdot,y)$ *are coercive.*

Analogous to [5, Theorem 3.1], we show that a stationary point of problem (3), it is also a critical point of problem (1). A point $\overline{x}\in\mathbb{R}^n$ is called a critical point of problem (1) if $\partial p(\overline{x})\cap\partial q(\overline{x})\neq\emptyset$.

Proposition 2. *Let Assumption I hold. If* $\overline{x}\in\mathbb{R}^n$ *is a stationary point of problem* (3) *and* $\nabla^2h(\overline{x})\succ 0$*, then* $\widehat{x}=\operatorname{prox}^h_{\gamma p}(\overline{x})$ *is a critical point of problem* (1)*. Moreover,* $f(\widehat{x})=p^h_\gamma(\overline{x})-q^h_\gamma(\overline{x})$*.*

Proof. It follows from Fact 1 (b) that

$$-\tfrac{1}{\gamma}\nabla^2h(\overline{x})\big(\overline{x}-\operatorname{prox}^h_{\gamma p}(\overline{x})\big)=-\tfrac{1}{\gamma}\nabla^2h(\overline{x})\big(\overline{x}-\operatorname{prox}^h_{\gamma q}(\overline{x})\big),$$

which implies $\operatorname{prox}^h_{\gamma p}(\overline{x})=\operatorname{prox}^h_{\gamma q}(\overline{x})$ as $\nabla^2h(\overline{x})\succ 0$. Hence, by from Fact 1 (d) we obtain

$$-\tfrac{1}{\gamma}(\nabla h(\widehat{x})-\nabla h(\overline{x}))\in\partial p(\widehat{x}),\quad -\tfrac{1}{\gamma}(\nabla h(\widehat{x})-\nabla h(\overline{x}))\in\partial q(\widehat{x}).$$

Consequently, $\partial p(\widehat{x})\cap\partial q(\widehat{x})\neq\emptyset$. It is readily seen that $f(\widehat{x})=p^h_\gamma(\overline{x})-q^h_\gamma(\overline{x})$, verifying the claim. □

The following proposition examines the converse of Proposition 2.

Proposition 3. *Let Assumptions I hold. If* $\overline{x}\in\mathbb{R}^n$ *is a critical point of problem* (1)*, then for all* $\xi\in\partial p(\overline{x})\cap\partial q(\overline{x})$ *with* $\gamma\xi+\nabla h(\overline{x})\in\operatorname{int}\operatorname{dom}h^*$*,* $\widehat{x}=\nabla h^*(\gamma\xi+\nabla h(\overline{x}))$ *is a stationary point of problem* (3)*. Moreover,* $f(\overline{x})=p^h_\gamma(\widehat{x})-q^h_\gamma(\widehat{x})$*.*

Proof. The proof follows from Fact 1. □

One may ask how local minimizers of problems (1) and (3) are related. In general, if $\overline{x}$ is a local minimizer of problem (3), then $\widehat{x} = \operatorname{prox}^h_{\gamma p}(\overline{x})$ is not necessarily a local minimizer of problem (1). To illustrate this, consider the following example.

Example 1. Consider optimization problem (1) where $p(x) = \max\{x^2, |x|\}$ and $q(x) = 2|x|$. Note that p and q are convex functions. Corresponding to the problem, we consider Moreau envelope reformulation 3 with $h(\cdot) = \frac{1}{2}|\cdot|$ and parameter $\gamma = 1$ where

$$q^h_\gamma(x) = \begin{cases} \frac{1}{2}x^2 & |x| \le 2, \\ 2|x| - 2 & |x| > 2, \end{cases} \qquad p^h_\gamma(x) = \begin{cases} \frac{1}{2}x^2 & |x| \le 1, \\ |x| - \frac{1}{2} & 1 < |x| \le 2, \\ 1 + \frac{1}{2}(|x| - 1)^2 & 2 < |x| \le 3, \\ \frac{1}{3}x^2 & |x| > 3. \end{cases}$$

It is seen that $\overline{x} = 0$ is a local minimizer of Moreau envelope reformulation 3 while $\widehat{x} = \operatorname{prox}_p(\overline{x}) = 0$ is a strict local maximizer of the original problem; see Figure 1. □

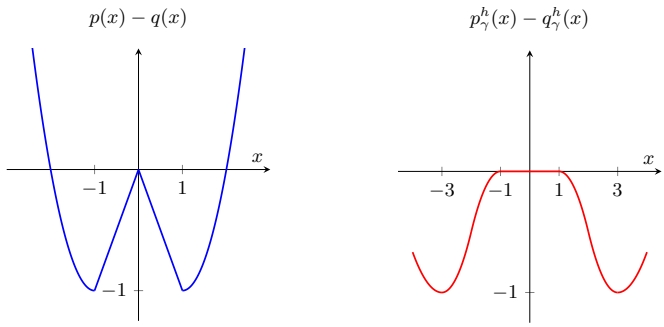

Fig. 1: Illustration of Example 1.

In what follows we show that Proportion 3 holds for local minimums.

Proposition 4. *Let Assumption I hold. If $\overline{x} \in \mathbb{R}^n$ is a local minimizer of problem (1), then for every $\xi \in \partial p(\overline{x}) \cap \partial q(\overline{x})$ such that $\gamma\xi + \nabla h(\overline{x}) \in \operatorname{int}\operatorname{dom} h^*$, the point $\widehat{x} := \nabla h^*(\gamma\xi + \nabla h(\overline{x}))$ is a local minimizer of problem (3).*

Proof. Since $\overline{x}$ is a local minimizer of problem (1), there exists $r > 0$ such that

$$\overline{f}(x) \le f(x), \forall x \in B(\overline{x}, r).$$

By [3, Proposition 3.10], the mapping $\mathrm{prox}^h_{\gamma p}$ is continuous at $\widehat{x}$ and satisfies

$$\mathrm{prox}^h_{\gamma p}(\widehat{x}) = \overline{x}.$$

Therefore, there exists $\delta > 0$ such that

$$\left\|\mathrm{prox}^h_{\gamma p}(x) - \overline{x}\right\| < r, \qquad \forall x \in B(\widehat{x}, \delta).$$

For any $x \in B(\widehat{x}, \delta)$, we have

$$p^h_\gamma(x) - q^h_\gamma(x) \geq p(p^h_\gamma(x)) + \mathrm{D}_h(p^h_\gamma(x), x) - q(p^h_\gamma(x)) - \mathrm{D}_h(p^h_\gamma(x), x) \geq p^h_\gamma(\widehat{x}) - q^h_\gamma(\widehat{x}),$$

where the second inequality follows from the local minimality of $\overline{x}$. This shows that $\widehat{x}$ is a local minimizer of problem (3), completing the proof. □

References

1. Astorino, A., Fuduli, A., Gaudioso, M.: Margin maximization in spherical separation. Comput. Optim. Appl. **53**(2), 301–322 (2012)
2. Bauschke, H.H., Dao, M.N., Lindstrom, S.B.: Regularizing with Bregman–Moreau envelopes. SIAM Journal on Optimization **28**, 3208–3228 (2018)
3. Bauschke, H.H., Combettes, P.L., Noll, D.: Joint minimization with alternating Bregman proximity operators. Pacific Journal of Optimization (2006)
4. Hartman, P.: On functions representable as a difference of convex functions. Pac. J. Math. **9**(3), 707–713 (1959)
5. Hiriart-Urruty, J.-B.: How to regularize a difference of convex functions. Journal of Mathematical Analysis and Applications **162**, 196–209 (1991)
6. Kan, C., Song, W.: The Moreau envelope function and proximal mapping in the sense of the Bregman distance. Nonlinear Analysis: Theory, Methods & Applications **75**, 1385–1399 (2012)
7. Lou, Y., Zeng, T., Osher, S., Xin, J.: A weighted difference of anisotropic and isotropic total variation model for image processing. SIAM J. Imag. Sci. **8**(3), 1798–1823 (2015)
8. Melzer, D.: On the expressibility of piecewise-linear continuous functions as the difference of two piecewise-linear convex functions. In: Demyanov, V.F., Dixon, L.C.W. (eds.) *Quasidifferential Calculus*. Mathematical Programming Studies, vol. 29. Springer, Berlin, Heidelberg (1986)
9. Rockafellar, R.T.: Convex Analysis. Princeton University Press, Princeton (1970)
10. Sun, K., Sun, X. A.: Algorithms for difference-of-convex programs based on difference-of-Moreau-envelopes smoothing. INFORMS J. Optim. **5**(4), 321–339 (2023)
11. Themelis, A., Hermans, B., Patrinos, P.: A new envelope function for nonsmooth DC optimization. In: Proceedings of the 59th IEEE Conference on Decision and Control, pp. 4697–4702. IEEE, New York (2020)
12. Toland, J.F.: Duality in nonconvex optimization. Journal of Mathematical Analysis and Applications **66**, 399–415 (1978)

Bounds and exact values of some domination parameters on cylindrical graphs

Janez Žerovnik[1,2]

[1] Rudolfovo - Science and Technology Centre Novo mesto, Slovenia
[2] Faculty of Mechanical Engineering, University of Ljubljana, Slovenia
janez.zerovnik@rudolfovo.eu, janez.zerovnik@fs.uni-lj.si

Abstract. Domination is among the most popular topics in graph theory, both due to its combinatiorial appeal and a number of practical applications.
Cylindrical graphs are naturally constructed from subgraphs of the infinite grid by certain identifications of boundary vertices. Considering various domination type problems, it is usually possible to find an optimal solution on the infinite grid. To the contrary, exact values of invariants for the cylindrical are typically only known for special subfamilies, and are in general hard to compute.
Here we recall recent results on the weak k-domination number, k-domination number, k-rainbow domination number, and singleton k-rainbow domination number, for $k = 2$ and $k = 4$, and discuss a possible approach to handle the missing case $k = 3$ that seems to be the hardest. Note that $k > 4$ is of less interest because the maximal degree of a cylindrial graph is 4.

Keywords: graph theory · rainbow domination · grid graphs

1 Introduction

Domination is among the most studied topics in graph theory [11, 12]. There are many variations extensively studied in the literature. Here we are interested in four of them including k-domination, k-rainbow domination, singleton k-rainbow domination, and weak k-domination. Two among them are well-known and are amog the most popular variations of graph domination. The first, k-domination has been studied in the literature for a long time [5]. More recently, k-rainbow domination problem was put forward in [2], also see [1]. Singleton k-rainbow domination [4] and weak k-domination are less popular, but as they are strongly related to the first two they are considered here as auxiliary notions that may help to clarify some interesting relations. To avoid possible confusion note that weak k-domination is a natural generalization of 2-domination as defined in [2], and it is not the weak domination as defined in [16]. Weak 2-domination is also known as Italian domination [13].

Cylindrical graphs, or cylindrical grid graphs, are Cartesian products of a path and a cycle. Domination number of cylindrical graphs has been studied in

[15, 3] and [9]. Recently, a lower bound for the 2-domination number of cylindrical graphs was proven in [14]. The computation of the 2-domination number of cylindrical graphs for arbitrary paths and small cylinders was addressed in [8], and for cylinders with small paths and arbitrary cycles in [7]. Domination numbers for 2-domination, 2-rainbow domination, singleton 2-rainbow domination, and weak 2-domination of cylindrical graphs were studied in [17]. For a recent brief outline of related previous work we refer to [17]. The case $k = 4$ is much less studied. In [6], it is shown that $\gamma_{r4}(P_m \Box C_3) = 2m$ and $\gamma_{r4}(P_3 \Box C_n) = 2n$. Domination numbers for 4-domination, 4-rainbow domination, singleton 4-rainbow domination, and weak 4-domination are studied in [18] providing analogous results to those for $k = 2$ given in [17].

As vertices in grid graphs are of degree at most four, the interesting k are 2,3, and 4. Below we recall the results for $k = 2$ and 4, and initiate the study of the missing case $k = 3$. We also discuss briefly the extension to $k > 4$. Details and formal proofs will appear in the full paper.

2 Definitions

A finite, simple and undirected graph $G = (V(G), E(G))$ is given by a set of vertices $V(G)$ and a set of edges $E(G)$. Edges are pairs of vertices. As usual, the edge $\{i, j\} \in E(G)$ is shortly denoted by ij.

The Cartesian product of two graphs, $G \Box H$, is the graph with vertex set $V(G) \times V(H)$, in which two vertices are adjacent if and only if they are equal in one coordinate and adjacent in the other. The Cartesian product of graphs is one of the standard graph products [10]. The Cartesian product is commutative. In other words: $G \Box H$ is isomorphic to $H \Box G$. In Cartesian product, copies of each factor appear as subgraphs and are called layers. In $G \Box H$, there are $|V(G)|$ isomorphic copies of H and $|V(H)|$ isomorphic copies of G. Here we are mainly interested in *cylindrical graphs* that are Cartesian products of a path and a cycle, $P_m \Box C_n$.

A set of vertices S is a *dominating set* of G if every vertex in the complement $V(G) \setminus S$ is adjacent to a vertex in S. The minimum cardinality of a dominating set of G is called the *domination number*, $\gamma(G)$. There are many variations of the basic domination, see e.g. [12].

Variations of domination A *k-dominating set* D is a set of vertices such that each vertex not in the set has at least two neighbors in the set. The *k-domination number* $\gamma_k(G)$ is the number of vertices in a smallest k-dominating set for G. A *k-rainbow dominating function* (kRDF) f of G assigns subsets of $\{1, 2, \ldots, k\}$ to vertices, such that for vertex v with $f(v) = \emptyset$, $\bigcup_{u \in N(v)} f(u) = \{1, 2, \ldots, k\}$. The *weight* $w(f)$ of kRDF f is $w(f) = \sum_{v \in V(G)} |f(v)|$. The minimum weight of a kRDF of G is the *k-rainbow domination number* denoted by $\gamma_{rk}(G)$.

An interesting special case are kRD functions that assign only singletons and empty sets. Such functions are called *singleton kRD functions* (SkRDF) and the

minimal weight obtained when considering only SkRD functions is the *singleton k-rainbow domination number*, $\tilde{\gamma}_{rt}$ [4]. Clearly, $\gamma_{rk} \leq \tilde{\gamma}_{rk}$.

Weak 2-domination was introduced in [2] as an auxiliary notion in the study of 2-rainbow domination on trees. Straightforward generalization to arbitrary k (the original definition is obtained by taking $k = 2$) is as follows. A function $f : V(G) \to \{0, 1, 2, \ldots, k\}$ is called a *weak k-domination* function (W2DF) if it has the following property. For any vertex with $f(v) = 0$ it holds $\sum_{u \in N(v)} f(u) \geq k$. The *weight* of f is $w(f) = \sum_{v \in V} f(v)$ and the *weak k-domination number* of G, $\gamma_{wk}(G)$, is the minimum weight over all WkDF of G. Obviously, any k-rainbow domination function f gives rise to a weak k-domination function w defined as $w(v) = |f(v)|$. In words, $w(v)$ is the cardinality of the set of colors assigned by f. Thus clearly $\gamma_{wk} \leq \gamma_{rk}$.

Furthermore, it is straightforward to see that weak k-domination is also a relaxation of k-domination as any k-domination function is also a weak k-domination function. On the other hand, a weak k-domination function is a k-domination function only if $f(v) \leq 1$ for all $v \in V$. Consequently, $\gamma_{wk} \leq \gamma_k$.

Similarly, any singleton k-rainbow domination function is a k-domination function, while the opposite is not true in general, so we have $\gamma_k \leq \tilde{\gamma}_{rk}$ [4].

Summarizing, we have the inequalities

$$\gamma_{wk}(G) \leq \gamma_{rk}(G) \leq \tilde{\gamma}_{rk}(G) \qquad \text{and} \qquad \gamma_{wk}(G) \leq \gamma_k(G) \leq \tilde{\gamma}_{rk}(G)\,.$$

3 Recent results on varieties including 2-rainbow and 4-rainbow domination on cylindrical graphs

Case $k = 2$. A constructive proof of the upper bound for singleton 2-rainbow domination is provided in [17] giving the upper bound

$$\gamma_{r2}(P_m \Box C_n)) \leq (m+2)\left\lfloor \frac{n}{3} \right\rfloor + (n^2 \bmod 3)m\,. \tag{1}$$

On the other hand, we have the lower bound for weak 2-domination

$$\gamma_{w2}(P_m \Box C_n)) \geq \frac{(m+2)m}{3}\,. \tag{2}$$

These two bounds, together with the inequalities among the domination varieties give us improved upper and lower bounds for cylindrical graphs. In some cases, exact values are obtained.

Theorem 1. *[17] For $m \geq 4$ and $n \equiv 0 \pmod 3$, $\gamma_{w2}(P_m \Box C_n)) =$*

$$= \gamma_2(P_m \Box C_n)) = \gamma_{r2}(P_m \Box C_n)) = \tilde{\gamma}_{r2}(P_m \Box C_n)) = \frac{(m+2)n}{3}\,. \tag{3}$$

The bounds are summarized in the next theorems. We write them as separate assertions to emphasize the possible independent importance of each of them.

Theorem 2. *[17] For $m \geq 4$ and $n \geq 3$. Then for the 2-domination mumber of cylindrical graph $\gamma_2(P_m \Box C_n))$ we have*

$$\frac{(m+2)n}{3} \leq \gamma_2(P_m \Box C_n)) \leq (m+2)\left\lfloor \frac{n}{3} \right\rfloor + (n^2 \bmod 3)m$$

Theorem 3. *[17] For $m \geq 4$ and $n \geq 3$. Then for the 2-rainbow domination mumber of cylindrical graph $\gamma_2(P_m \Box C_n))$ we have*

$$\frac{(m+2)n}{3} \leq \gamma_{r2}(P_m \Box C_n)) \leq (m+2)\left\lfloor \frac{n}{3} \right\rfloor + (n^2 \bmod 3)m$$

Theorem 4. *[17] For $m \geq 4$ and $n \geq 3$. Then for the singleton 2-rainbow domination mumber of cylindrical graph $\tilde{\gamma}_2(P_m \Box C_n))$ we have*

$$\frac{(m+2)n}{3} \leq \tilde{\gamma}_{r2}(P_m \Box C_n)) \leq (m+2)\left\lfloor \frac{n}{3} \right\rfloor + (n^2 \bmod 3)m$$

Theorem 5. *[17] For $m \geq 4$ and $n \geq 3$. Then for the weak 2-domination mumber of cylindrical graph $\tilde{\gamma}_2(P_m \Box C_n))$ we have*

$$\frac{(m+2)n}{3} \leq \gamma_{w2}(P_m \Box C_n)) \leq (m+2)\left\lfloor \frac{n}{3} \right\rfloor + (n^2 \bmod 3)m$$

Case $k = 4$. Analogous results for $k = 4$ appear in [18], in particular, we have the following results.

Theorem 6. *[18] For $m, n \geq 3$ it holds*

$$\frac{(m+1)n}{2} \leq \gamma_{w4}(P_m \Box C_n)) \leq \begin{cases} \frac{(m+1)n}{2}, & n \equiv 0 \pmod 4 \\ \frac{(m+1)(n+1)}{2} + 1, & n \equiv 1 \pmod 4 \\ \frac{(m+1)n}{2} + 1, & n \equiv 2 \pmod 4 \\ \frac{(m+1)(n+1)}{2}, & n \equiv 3 \pmod 4 \end{cases} \tag{4}$$

Corollary 1. *For $m \geq 3$ and $n \equiv 0 \pmod 4$, $\gamma_{w4}(P_m \Box C_n)) = \frac{(m+1)n}{2}$.*

Theorem 7. *[18] For $m \geq 3$, $n \geq 4$ it holds*

$$\frac{(m+2)n}{2} \leq \gamma_4(P_m \Box C_n)) \leq \tilde{\gamma}_{r4}(P_m \Box C_n)) \leq \begin{cases} \frac{(m+2)n}{2}, & n \equiv 0 \pmod 4 \\ \frac{(m+2)(n+1)}{2}, & n \equiv 1, 3 \pmod 4 \\ \frac{(m+2)(n+2)}{2}, & n \equiv 2 \pmod 4 \end{cases} \tag{5}$$

Corollary 2. *For $m \geq 3$ and $n \equiv 0 \pmod 4$, $\tilde{\gamma}_{r4}(P_m \Box C_n)) = \gamma_4(P_m \Box C_n)) = \frac{(m+2)n}{2}$.*

Theorem 8. *[18] For $m, n \geq 3$ it holds*

$$\frac{(m+1)n}{2} \leq \gamma_{r4}(P_m \Box C_n)) \leq \begin{cases} \frac{(m+2)n}{2}, & n \equiv 0 \pmod 4 \\ \frac{(m+2)(n+1)}{2}, & n \equiv 1,3 \pmod 4 \\ \frac{(m+2)(n+2)}{2}, & n \equiv 2 \pmod 4 \end{cases} \quad (6)$$

Remark. Note that there is a significant gap between the two bounds for the 4-rainbow domination number γ_{r4}. However, the example provided in [6], namely $\gamma_{r4}(P_m \Box C_3)) = 2m$ shows that the lower bound is tight indicating that the lower bound may give exact values in some other cases as well.

4 The missing cases: $k = 3$ and $k > 4$

The case $k = 3$ appears to be somewhat more challenging. Regarding the upper bounds, we note here that we can adapt the constructions for $k = 2$ and for $k = 4$ to obtain the upper bounds for the case $k = 3$. The first upper bound is based on Theorem 3, where in the construction, one of the colors, say "2" is replaced with the set of colors $\{2, 3\}$. Note however that even if we have started with a singleton rainbow domination function, the result is NOT a sigleton fuction. On the positive side, observe that we can assume that the the chosen color is used at most haf of the time, thus factor $\frac{3}{2}$ for the weight of the resulting assignment.

Theorem 9. *For $m \geq 4$ and $n \geq 3$. Then for the 3-rainbow domination mumber of cylindrical graph $\gamma_3(P_m \Box C_n))$ we have*

$$\gamma_{w3}(P_m \Box C_n)) \leq \gamma_{r3}(P_m \Box C_n)) \leq \frac{3}{2}\left((m+2)\left\lfloor \frac{n}{3} \right\rfloor + (n^2 \bmod 3)m\right)$$

The second upper bound is more general as applies to singleton 3-rainbow domination. Start with construction used in the proof of Theorem , where we identify colors 3 and 4. Obviously, a 3-rainbow domination function is obtained. Each vertex is assigned at most one color, hoewver, the vertices have two neighbors colored with color 3, and therefore the assignment may not be best possible.

Theorem 10. *For $m \geq 3$, $n \geq 4$ it holds $\gamma_{w3}(P_m \Box C_n)) \leq \gamma_3(P_m \Box C_n)) \leq$*

$$\leq \tilde{\gamma}_{r3}(P_m \Box C_n)) \leq \begin{cases} \frac{(m+2)n}{2}, & n \equiv 0 \pmod 4 \\ \frac{(m+2)(n+1)}{2}, & n \equiv 1,3 \pmod 4 \\ \frac{(m+2)(n+2)}{2}, & n \equiv 2 \pmod 4 \end{cases} \quad (7)$$

Each of the two upper bounds in the two theorems is a better approximation of $\gamma_{r3}(P_m \Box C_n)$ in special cases, compare for example the cases ($n \equiv 0 \pmod 3$ and $n \equiv 0 \pmod 4$). It remains open whether a significantly better upper bound can be obtained, i.e. is there a constant $C < \frac{1}{2}$ such that $\gamma_{r3}(P_m \Box C_n) \leq C(m+2)n$?

For $k > 4$, singleton k-rainbow domination functions do not exist. Fro some $k > 4$, it is however possible to study $\gamma_{rk}(P_m \Box C_n)$, for example with the constructions for $k = 2, 3$ and 4, are used and the colors are replaced with sets of colors.

References

1. B. Brešar. Rainbow domination in graphs. In T. W. Haynes, S. T. Hedetniemi, and M. A. Henning, editors, *Topics in Domination in Graphs*, pages 411 – 443. Springer International Publishing, Cham, 2020.
2. B. Brešar, M. A. Henning, and D. F. Rall. Rainbow domination in graphs. *Taiwanese Journal of Mathematics*, 12(1):213 – 225, 2008.
3. J. J. Carreno, J. A. Martinez, and M. L. Puertas. A general lower bound for the domination number of cylindrical graphs. *ulletin of the Malaysian Mathematical Sciences Society*, 43(2):1671, 2020.
4. R. Erveš and J. Žerovnik. On 3-rainbow domination number of generalized Petersen graphs $P(6k, k)$. *Symmetry*, 13(10), 2021.
5. J. F. Fink and M. S. Jacobson. n-domination in graphs. In *Graph Theory with Application to Algorithms and Computer Science*, 1985.
6. H. Gao, Y. Zhang, Y. Wang, Y. Guo, X. Liu, R. Liu, C. Xi, and Y. Yang. Rainbow domination in cartesian product of paths and cycles. *International Journal of Foundations of Computer Science*, 35(08):907–928, 2024.
7. E. M. Garzón, J. A. Martínez, J. J. Moreno, and M. L. Puertas. Hpc acceleration of large (min, +) matrix products to compute domination-type parameters in graphs. *The Journal of Supercomputing*, 78(16):17826–17843, 2022.
8. E. M. Garzón, J. A. Martínez, J. J. Moreno, and M. L. Puertas. On the 2-domination number of cylinders with small cycles. *Fundamenta Informaticae*, 185(2):185–199, 2022.
9. D. R. Guichard. A new lower bound for the domination number of complete cylindrical grid graphs. *Journal of Combinatorial Mathematics and Combinatorial Computing*, 120:411–416, 2024.
10. R. Hammack, W. Imrich, and S. Klavžar. *Handbook of product graphs*. Discrete Mathematics and its Applications (Boca Raton). CRC Press, Boca Raton, FL, second edition, 2011.
11. T. Haynes, S. Hedetniemi, and P. Slater. *Fundamentals of Domination in Graphs*. CRC Press, New York, 1st ed. edition, 1998.
12. T. W. Haynes, S. T. Hedetniemi, and M. A. Henning. *Topics in Domination in Graphs*. Springer International Publishing, Cham, 2020.
13. W. F. Klostermeyer and G. MacGillivray. Roman, italian, and 2-domination. *Journal of Combinatorial Mathematics and Combinatorial Computing*, 108:125–146, 2019.
14. J. A. Martínez, A. B. Castano-Fernandez, and M. L. Puertas. The 2-domination number of cylindrical graphs. *Computational and Applied Mathematics*, 41(8):424, 2022.
15. M. Nandi, S. Parui, and A. Adhikari. The domination numbers of cylindrical grid graphs. *Applied Mathematics and Computation*, 217(10):4879–4889, 2011.
16. E. Sampathkumar and L. Latha. Strong weak domination and domination balance in a graph. *Discrete Mathematics*, 161(1):235–242, 1996.
17. J. Žerovnik. On 2-domination and 2-rainbow domination of cylindrical graphs. *Computational and Applied Mathematics*, 44(5):293, 2025.
18. J. Žerovnik. On 4-domination and 4-rainbow domination of cylindrical graphs. *Communications in Combinatorics and Optimization*, in press, 2025.